Finite Elements in Analysis and Design 251 (2025) 104433

Contents lists available at ScienceDirect

Finite Elements in Analysis & Design

journal homepage: www.elsevier.com/locate/finel

A pure-Lagrangian finite element approach for solving thermo-electrical-mechanical models. Application to electric upsetting

M. Benítez [a,b], A. Bermúdez [a,c], P. Fontán [d], I. Martínez [a,c,*], P. Salgado [a,c]

[a] Centro de Investigación e Tecnoloxía Matemática de Galicia (CITMAga), E-15782 Santiago de Compostela, Spain
[b] Departamento de Matemáticas, Universidade da Coruña, r/ da Fraga, 27, E-15008 A Coruña, Spain
[c] Departamento de Matemática Aplicada, Universidade de Santiago de Compostela, r/ Lope Gómez de Marzoa s/n, E-15782 Santiago de Compostela, Spain
[d] REPSOL Technology Lab, Autovía de Extremadura s/n, E-28935 Móstoles, Madrid, Spain

ARTICLE INFO

Keywords:
Thermo-electrical-mechanical
Large deformations
Time dependent domain
Pure-Lagrange–Galerkin methods
High order schemes
Electric upsetting

ABSTRACT

In this paper, we introduce a novel numerical procedure for solving fully coupled thermo-electrical-mechanical problems using implicit Runge–Kutta time integration within a purely Lagrangian finite element framework. Our formulation, grounded in continuum mechanics, accurately captures the interdependence of mechanical, thermal, and electrical effects under large deformations. It features a fully coupled thermo-electrical-mechanical Lagrangian model with an elasto-viscoplastic constitutive law, considers six primary variables –velocity, temperature, electric potential, plastic deformation gradient, an internal strain hardening variable, and a Lagrange multiplier for enforcing contact conditions– and employs a pure-Lagrangian description. This ensures the computational domain remains fixed and known a priori, simplifies the tracking of free surfaces, and eliminates convective terms. To validate our approach, we solve several axisymmetric benchmark problems and analyze convergence rates in both time and space. Moreover, our numerical results show excellent agreement with the solution obtained using commercial packages for an in-die electric upsetting process.

1. Introduction

Electrically Assisted Forming (EAF) is a technique that applies electricity, in the form of direct or alternating current, to a metallic workpiece to enhance its formability during deformation. This relatively recent technique has received significant industrial interest due to its ability to substantially reduce the flow stress of metallic materials during deformation. It is considered a promising method for manufacturing lightweight structures, particularly in the automotive and aerospace industries. The application of electric current generates heat which alters the mechanical behaviour of materials under electrically assisted deformation, often resulting in an elasto-viscoplastic response in metals. In this paper, we will limit ourselves to direct current sources.

The EAF process is highly complex, involving an interplay of electrical, thermal, and mechanical phenomena. Electrical currents generate heat, which alters the properties of the material, such as its mechanical strength. Temperature significantly influences the mechanical constitutive behaviour and electrical conductivity, while the domain of the workpiece evolves over

* Corresponding author at: Departamento de Matemática Aplicada, Universidade de Santiago de Compostela, r/ Lope Gómez de Marzoa s/n, E-15782 Santiago de Compostela, Spain.
E-mail addresses: marta.benitez@udc.es (M. Benítez), alfredo.bermudez@usc.es (A. Bermúdez), pfontan@gmail.com (P. Fontán), ivanmartinez.suarez@usc.es (I. Martínez), mpilar.salgado@usc.es (P. Salgado).

https://doi.org/10.1016/j.finel.2025.104433
Received 3 July 2025; Received in revised form 1 August 2025; Accepted 10 August 2025
Available online 28 August 2025

time due to deformations. Consequently, accurately modeling the EAF process requires a multiphysics approach that captures large deformations, heat generation from electromagnetic fields, and the strong temperature dependence of electrical, thermal, and mechanical properties. Additionally, mechanical contact between components, such as a die guiding the preforming target, must be considered.

Computing approximations of the solutions of these (fully coupled) problems presents significant challenges, which requires development of reliable and accurate numerical methods. This paper contributes to the development of numerical techniques for multiphysics coupling models and numerical simulations of EAF processes, with a specific focus on electric upsetting. This preforming technique creates a localized enlargement at one end of a metallic bar, which can then be forged without additional heating. Numerical solutions for electric upsetting problems are often derived from commercial codes, as in [1,2], where the mathematical and numerical models are not presented in detail. In this paper, we develop and solve a fully coupled thermo-electrical-mechanical model for large-deformation electric upsetting driven by DC sources. For this purpose, we introduce novel numerical strategies based on a pure-Lagrangian formulation, tailored to address the specific challenges of this class of problems, namely, mesh distortion, complex material motion, and the strong interplay among thermal, electrical, and mechanical fields.

A unified pure-Lagrangian approach is employed to solve the three fully coupled problems: electrical, thermal, and mechanical. To better discuss the relevance of our efforts towards devising this type of scheme, we briefly review the development of characteristics-based methods, extensively used for solving convection-diffusion problems dominated by convection (see the review paper [3]). These methods are based on the time discretization of the time derivative along characteristic curves. When they are referred to a fixed domain (respectively, to a time-dependent domain), they are called pure-Lagrangian methods (respectively, semi-Lagrangian methods). Combined with finite element methods, they are often called Lagrange–Galerkin methods. Classical methods of characteristics, formulated in Eulerian coordinates, have been mathematically analyzed and applied to different problems over time-independent domains by several authors (e.g., [4–10]). Higher-order schemes for time discretization along characteristic curves enhance time accuracy (see [4,5,9]).

In solid mechanics, numerical models are typically based on a Lagrangian formulation, in contrast to the Eulerian approach commonly used for fluid mechanics, thermo-electrical or electromagnetic problems. Traditional difficulties of the Eulerian description include the treatment of convective terms and the modelling and tracking of free surfaces, which disappear in the Lagrangian framework. Pure-Lagrangian methods present additional advantages, including a time-independent and predefined computational domain, higher accuracy in regions of strong gradients or discontinuities of the solution, and the absence of error terms involving the time step in the denominator, which are common in semi-Lagrangian methods. However, due to the significant distortion of the moving mesh, remeshing and reinitialization may periodically be required. Methods derived from this Lagrangian framework belong to the class of characteristics-based methods.

Recent contributions by some of the present authors include the development of Lagrange–Galerkin methods to solve convection-diffusion equations with time dependent domains, first for scalar linear problems (see [11–13]) and then for nonlinear vector ones (see [14–16]). Most of these methods are linear and all of them are obtained by introducing a change of variable from the current configuration to a reference configuration (known) and employ high-order time discretizations. Unified formulations to state pure-Lagrangian and semi-Lagrangian methods have been proposed for both scalar and vector convection-diffusion problems [13,14,16]. Additionally, a first step based on Lagrangian approaches in the context of electric upsetting was made in [17] for solving a thermo-electromagnetic problem, but with known time-dependent domains and alternating current sources.

In electric upsetting simulations, sequential multiphysics algorithms –often using updated Lagrangian or Eulerian formulations– are commonly employed; see, for example, [2]. The updated Lagrangian approach incrementally deforms the mesh using the previous configuration, whereas Eulerian methods require regenerating the computational domain at each time step. In contrast, we adopt a purely Lagrangian formulation for all coupled physics, expressing discrete equations in the reference configuration. This eliminates the need for remeshing at each step and provides a unified framework for thermo-electro-mechanical coupling. It is worth noting that related Lagrangian formulations for coupled thermo-electromagnetic-mechanical problems have been explored previously, notably in [18], which addressed these challenges in the context of medical EAF applications.

Based on a Lagrangian framework as that introduced in [18], this work extends it in several key directions to tackle the specific challenges of electric upsetting processes. First, we introduce high-order Runge–Kutta time integration schemes into our framework, vastly improving temporal accuracy compared to the first-order backward Euler method employed in [18]. Second, we replace the simpler elastoplastic constitutive model used in that prior work with a robust elasto-viscoplastic formulation suitable for large deformations, built upon the classic theoretical foundations in [19]. Additionally, we implement robust contact conditions and an axisymmetric formulation, both essential for accurately modeling electric upsetting. Employing consistent surface-to-surface contact in a purely Lagrangian axisymmetric setting ensures realistic interaction at the billet-anvil interface while preserving compatibility with cylindrical symmetry. Together, these contributions establish a unified, remesh-free Lagrangian simulation framework for coupled thermo-electro-mechanical problems, operating entirely in the reference configuration and naturally handling evolving geometries.

The paper is structured as follows: Section 2 describes the physical foundations of EAF thermo-electrical-mechanical processes. Section 3 formulates a general initial-boundary value thermo-electrical-mechanical problem in a time-dependent bounded domain (Eulerian), and recalls some hypotheses and notations concerning motion. Section 4 introduces a transformation to the reference configuration (Lagrangian), yielding a reformulated problem in a time-independent domain. The motion equation is complemented with an elasto-viscoplastic constitutive model for large deformations, and the associated weak Lagrangian formulations are derived. Section 5 focuses on axisymmetric formulations for typical domains of electric upsetting processes. Section 6 describes the fully discretized scheme, combining finite elements for spatial discretization with Runge–Kutta methods for time integration. Section 7 presents numerical examples illustrating the performance of the proposed method.

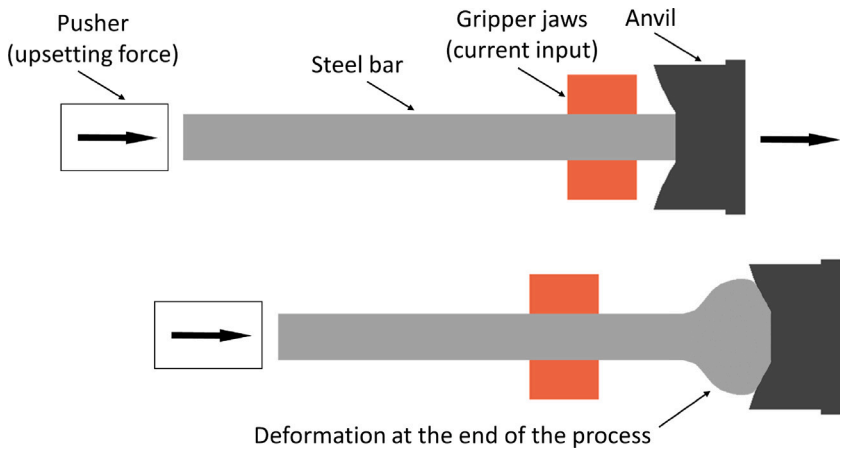

Fig. 1. Electric upsetting process.

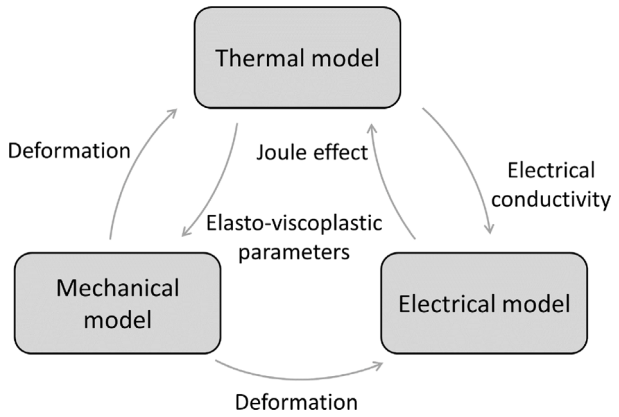

Fig. 2. Thermo-electrical-mechanical coupling.

2. Description of EAF thermo-electrical-mechanical processes

In EAF processes, electrical current flows through a workpiece, causing the material to heat up due to Joule effect, thereby reducing the force required to achieve the desired deformation. In the particular case of electric upsetting, a local enlarged diameter is created at one end of a metal bar, which is placed in a horizontal upsetting machine and clamped by gripper jaws. A high-amperage, low-voltage electrical current passes through the bar via contact between one of its ends and the gripper jaws, causing the bar end to heat up and exhibit a plastic behaviour. When enough temperature is reached, the bar is pushed against the anvil with the help of an upsetting force applied by a pusher located at the opposite end. As a consequence, the diameter at the hot end is enlarged. A sketch of the electric upsetting process is shown in Fig. 1.

The full simulation of electric upsetting involves coupled thermal, electrical, and mechanical phenomena, with the coupling influenced by several factors. Firstly, the deformation of the metal bar alters the computational domain for all models. Additionally, the electrical conductivity and the elasto-viscoplastic mechanical properties of the material are temperature-dependent, creating a coupling with the thermal model. Moreover, the heat source in the thermal model is associated with the power dissipated by the electrical current through the bar, known as the Joule effect. The coupling scheme is illustrated in Fig. 2.

Let us note that there are additional physical effects, such as thermal expansion and plastic heat dissipation, which are not considered in this work for the sake of simplicity, and because their influence on the electric upsetting processes under consideration is quite limited.

In the next section, the mechanical, electrical, and thermal submodels that constitute the fully coupled multiphysics problem are introduced.

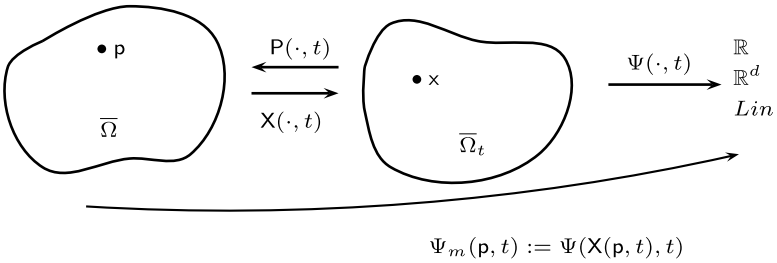

Fig. 3. Motion and material description of spatial fields.

3. Statement of the problem in Eulerian coordinates. General assumptions and notations

Let Ω be a bounded domain in $\mathbb{R}^d$ ($d = 2, 3$) with Lipschitz boundary Γ. Let $\mathsf{X} : \overline{\Omega} \times \mathbb{R} \longrightarrow \mathbb{R}^d$ be a *motion* defined as in Gurtin [20]. In particular, $\mathsf{X} \in \mathbf{C}^3(\overline{\Omega} \times \mathbb{R})$ and for each fixed $t \in \mathbb{R}$, $\mathsf{X}(\cdot, t)$ is a one-to-one function satisfying

$$\det \mathbf{F} > 0, \quad \text{in } \overline{\Omega} \times \mathbb{R}, \tag{1}$$

being $\mathbf{F}(\cdot, t)$ the Jacobian tensor of the deformation $\mathsf{X}(\cdot, t)$. For given $\mathcal{A} \subset \overline{\Omega}$, we denote $\mathcal{A}_t := \mathsf{X}(\mathcal{A}, t)$ (see Fig. 3). In practice, a bounded time interval is considered for the motion, namely, $[t_0, t_f]$, being t_0, t_f two non-negative numbers. We denote by p the *material points* in the *reference domain* $\overline{\Omega}$, by t the *current time* and by x the *spatial points* in $\overline{\Omega}_t$ with $t > t_0$. We notice that mapping $t \in [t_0, t_f] \to \mathsf{X}(\mathsf{p}, t) \in \overline{\Omega}_t$ describes the trajectory of a material point $\mathsf{p} \in \overline{\Omega}$. Accordingly, we introduce the *trajectory* of the motion as the set

$$\mathcal{T} = \{(\mathsf{x}, t) : \mathsf{x} \in \overline{\Omega}_t, \ t \in [t_0, t_f]\}. \tag{2}$$

For each t, $\mathsf{X}(\cdot, t)$ is a one-to-one mapping from $\overline{\Omega}$ onto $\overline{\Omega}_t$; hence it has an inverse

$$\mathsf{P}(\cdot, t) : \overline{\Omega}_t \longrightarrow \overline{\Omega} \tag{3}$$

such that

$$\mathsf{X}(\mathsf{P}(\mathsf{x}, t), t) = \mathsf{x}, \qquad \mathsf{P}(\mathsf{X}(\mathsf{p}, t), t) = \mathsf{p}, \quad \forall (\mathsf{x}, t) \in \mathcal{T}, \ \forall (\mathsf{p}, t) \in \overline{\Omega} \times [t_0, t_f]. \tag{4}$$

Notice that $\mathsf{x} = \mathsf{X}(\mathsf{p}, t)$ if and only if $\mathsf{p} = \mathsf{P}(\mathsf{x}, t)$. The mapping $\mathsf{P} : \mathcal{T} \longrightarrow \overline{\Omega}$, so defined is called the *reference map* of motion X and $\mathsf{P} \in \mathbf{C}^3(\mathcal{T})$ (see [20] pp. 65 – 66).

Fields defined in $\mathcal{T}$ (respectively, in $\overline{\Omega} \times [t_0, t_f]$) are called *spatial fields* (respectively, *material fields*). If Ψ is a spatial field, we define its *material description* Ψ_m by

$$\Psi_m(\mathsf{p}, t) := \Psi(\mathsf{X}(\mathsf{p}, t), t), \quad \forall (\mathsf{p}, t) \in \overline{\Omega} \times [t_0, t_f]. \tag{5}$$

This mapping is depicted in Fig. 3. Similar definition is used for functions, Ψ, whose domain is a subset of $\mathcal{T}$. For the sake of clarity, in expressions involving space and time derivatives we use the definitions and notation given in [20]. In particular, if Φ is a smooth material field, we denote by $\nabla\Phi$ (respectively, by $\mathrm{Div}\,\Phi$) the gradient (respectively, the divergence) with respect to the first argument (p), and by $\dot{\Phi}$ the partial derivative with respect to the second argument (time). Similarly, if Ψ is a smooth spatial field, we denote by $\mathrm{grad}\Psi$ (respectively, by $\mathrm{div}\Psi$) the gradient (respectively, the divergence) with respect to the first argument (x), and by Ψ' the partial derivative with respect to the second argument (time). In some places where these operators appear, we specify the differentiation variable as a subscript, e.g., $\nabla_{\mathsf{p}}\Phi$, $\mathrm{grad}_{\mathsf{x}}\Psi$ (respectively, $\mathrm{Div}_{\mathsf{p}}\,\Phi$, $\mathrm{div}_{\mathsf{x}}\Psi$) denote the gradient (respectively, the divergence) with respect to the first argument (p or x). Let us recall that the *spatial description* of the velocity $\mathbf{v} : \mathcal{T} \longrightarrow \mathbb{R}^d$ is defined by

$$\mathbf{v}(\mathsf{x}, t) := \dot{\mathsf{X}}(\mathsf{P}(\mathsf{x}, t), t), \quad \forall (\mathsf{x}, t) \in \mathcal{T}. \tag{6}$$

Moreover, we notice that, from the above definitions and by using the chain rule, we get

$$(\mathrm{grad}_{\mathsf{x}}\Psi)_m = \mathbf{F}^{-t}\nabla_{\mathsf{p}}\Psi_m, \tag{7}$$

for any smooth spatial scalar field Ψ.

If Ψ is a smooth spatial field, $\dot{\Psi}$ denotes the *material time derivative* with respect to time, that is,

$$\dot{\Psi}(\mathsf{x}, t) = \frac{\partial}{\partial t}\left(\Psi(\mathsf{X}(\mathsf{p}, t), t)\right)\Big|_{\mathsf{p}=\mathsf{P}(\mathsf{x},t)}, \quad \forall (\mathsf{x}, t) \in \mathcal{T}. \tag{8}$$

In particular, if Ψ is scalar valued, we have

$$\dot{\Psi} = \Psi' + \mathrm{grad}\Psi \cdot \mathbf{v}, \quad \text{in } \mathcal{T}, \tag{9}$$

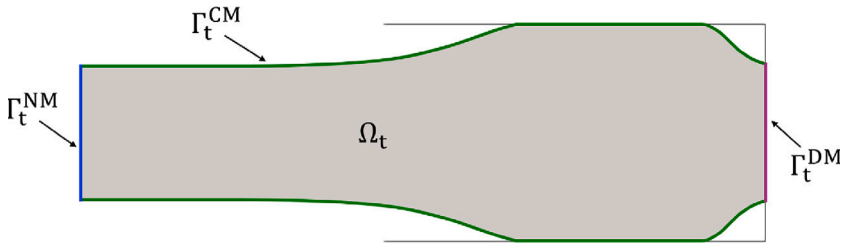

Fig. 4. Mechanical problem: boundary conditions.

where we have used the chain rule. A similar equation is obtained for a vector valued spatial field $\boldsymbol{\Psi}$, namely,

$$\dot{\boldsymbol{\Psi}} = \boldsymbol{\Psi}' + \mathrm{grad}\boldsymbol{\Psi}\mathbf{v}, \quad \text{in } \mathcal{T}. \tag{10}$$

Let us recall that the material displacement $\mathbf{u} : \overline{\Omega} \times [t_0, t_f] \longrightarrow \mathbb{R}^d$ is defined by

$$\mathbf{u}(\mathsf{p}, t) = \mathsf{X}(\mathsf{p}, t) - \mathsf{p},$$

for $(\mathsf{p}, t) \in \overline{\Omega} \times [t_0, t_f]$. Moreover, we denote by $\mathbf{u}_s : \mathcal{T} \longrightarrow \mathbb{R}^d$ the spatial displacement and by $\mathbf{a} : \mathcal{T} \longrightarrow \mathbb{R}^d$ the spatial acceleration, namely,

$$\mathbf{u}_s(\mathsf{x}, t) := \mathbf{u}(\mathsf{P}(\mathsf{x}, t), t), \quad \mathbf{a}(\mathsf{x}, t) = \ddot{\mathsf{X}}(\mathsf{p}, t)|_{\mathsf{p}=\mathsf{P}(\mathsf{x},t)}, \tag{11}$$

for $(\mathsf{x}, t) \in \mathcal{T}$. Then, by using the above definitions, we have

$$\mathbf{v}_m = \dot{\mathsf{X}} = \dot{\mathbf{u}}, \quad \mathbf{a}_m = \dot{\mathbf{v}}_m = \ddot{\mathsf{X}} = \ddot{\mathbf{u}}, \quad \text{in } \overline{\Omega} \times [t_0, t_f]. \tag{12}$$

We are going to consider the motion equation of continuum mechanics subjected to initial and mixed boundary conditions. Different boundary decompositions are considered depending on the effect to be modeled. Throughout this paper, boundary notation is defined using two superscripts: the first indicates the type of boundary condition (D: Dirichlet, N: Neumann, C: Contact and R: Robin), while the second refers to the specific submodel (M: Mechanical, E: Electrical and T: Thermal).

The deformation of the domain is computed from the mechanical model, which consists of the momentum balance equation in terms of the velocity field, in conjunction with adequate constitutive laws and boundary and initial conditions.

Regarding the mechanical problem, the boundary Γ_t is decomposed into three disjoint parts, $\Gamma_t = \Gamma_t^{DM} \cup \Gamma_t^{NM} \cup \Gamma_t^{CM}$ (see Fig. 4), and the displacement is given on Γ_t^{DM}, while a Neumann-like boundary condition is prescribed on Γ_t^{NM}.

In addition, we assume that deformation is restricted by a rigid obstacle occupying the (given) open set C which is assumed to be defined by a function M as follows:

$$\mathsf{C} = \{\mathsf{x} \in \mathbb{R}^d \, : \, M(\mathsf{x}) < 0\}, \tag{13}$$

being its boundary $\partial\mathsf{C} = \{\mathsf{x} \in \mathbb{R}^d \, : \, M(\mathsf{x}) = 0\}$. On the other hand, the part of the boundary susceptible to contact with the obstacle is Γ_t^{CM}, where a contact Lagrange multiplier is defined. Then, we consider the following initial-boundary value problem (motion equation of continuum mechanics).

Eulerian general mechanical problem (EGMP). *Find three mappings* $\mathbf{v} : \mathcal{T} \longrightarrow \mathbb{R}^d$ *(velocity),* $\mathbf{T} : \mathcal{T} \longrightarrow Lin$ *(Cauchy stress tensor) and* $\tilde{\zeta} : \bigcup_{t\in[t_0,t_f]} \Gamma_t^{CM} \times \{t\} \to \mathbb{R}$ *(contact Lagrange multiplier) such that*

$$\rho\mathbf{v}' + \rho\mathrm{grad}\mathbf{v}\mathbf{v} - \mathrm{div}\mathbf{T} = \mathbf{b}, \ \textit{in } \mathcal{T}, \tag{14}$$

subject to the boundary conditions

$$\mathbf{u}_s(\mathsf{x}, t) = \mathbf{u}_s^{\mathrm{D}}(\mathsf{x}, t), \quad \forall \mathsf{x} \in \Gamma_t^{DM}, \tag{15}$$

$$\mathbf{T}(\mathsf{x}, t)\mathbf{n}(\mathsf{x}, t) = \mathbf{h}(\mathsf{x}, t), \quad \forall \mathsf{x} \in \Gamma_t^{NM}, \tag{16}$$

$$\mathbf{T}(\mathsf{x}, t)\mathbf{n}(\mathsf{x}, t) = -\tilde{\zeta}(\mathsf{x}, t)\mathbf{n}(\mathsf{x}, t), \quad \forall \mathsf{x} \in \Gamma_t^{CM}, \tag{17}$$

$$M(\mathsf{x}) \geq 0, \quad \forall \mathsf{x} \in \Gamma_t^{CM}, \tag{18}$$

$$\tilde{\zeta}(\mathsf{x}, t) \geq 0, \quad \forall \mathsf{x} \in \Gamma_t^{CM}, \tag{19}$$

$$\tilde{\zeta}(\mathsf{x}, t)M(\mathsf{x}) = 0, \quad \forall \mathsf{x} \in \Gamma_t^{CM}, \tag{20}$$

for $t \in (t_0, t_f]$*, and to the initial condition*

$$\mathbf{v}(\mathsf{x}, t_0) = \mathbf{v}^0(\mathsf{x}), \quad \forall \mathsf{x} \in \overline{\Omega}_{t_0}. \tag{21}$$

In the above equations, Lin denotes the space of tensors in the d-dimensional space, $\rho : \mathcal{T} \longrightarrow \mathbb{R}$ (mass density), $\mathbf{b} : \mathcal{T} \longrightarrow \mathbb{R}^d$ (volumetric force density), $\mathbf{u}_s^D(\cdot, t) : \Gamma_t^{DM} \longrightarrow \mathbb{R}^d$ (displacement on Dirichlet boundary), $\mathbf{h}(\cdot, t) : \Gamma_t^{NM} \longrightarrow \mathbb{R}^d$ (surface force density)

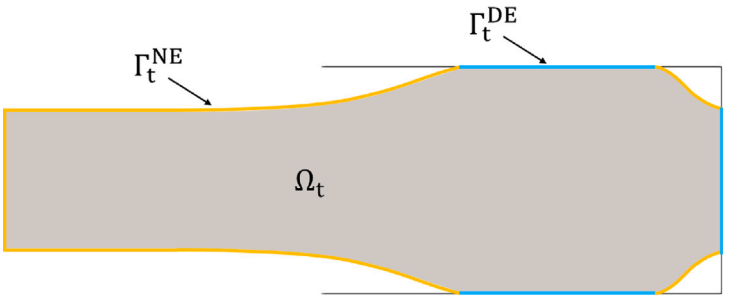

Fig. 5. Electrical problem: boundary conditions.

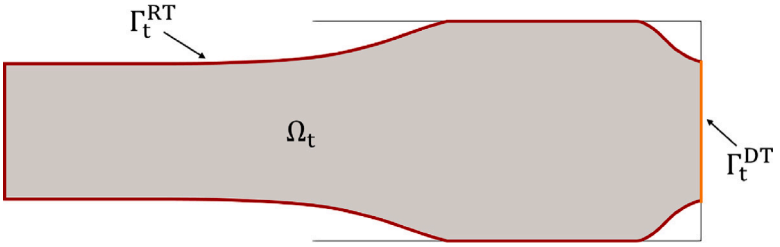

Fig. 6. Thermal problem: boundary conditions.

and $\mathbf{v}^0 : \overline{\Omega} \longrightarrow \mathbb{R}^d$ (initial velocity), $t \in (t_0, t_f]$, are given fields, $\mathbf{n}(\cdot, t)$ is the outward unit normal vector to Γ_t. The unilateral boundary conditions (17)–(20) correspond to contact without friction being the function $\tilde{\zeta}$ the Lagrange multiplier which takes care of the non-penetration constraint. Moreover, we note that in some cases the surface density of the surface load $\mathbf{h}(\mathrm{x}, t)$ is unknown; instead, the resultant force over Γ_t^{NM}, $\mathbf{P}(t)$, is given, that is,

$$\mathbf{P}(t) = \int_{\Gamma_t^{NM}} \mathbf{h}(\mathrm{x}, t)\, \mathrm{d}\, A_{\mathrm{x}}.$$

Notice that the system of equations given in (**EGMP**) is undetermined. In order to complete the above system, constitutive assumptions on the form of the Cauchy stress tensor $\mathbf{T}$ will be introduced in Section 4. These additional equations depend on the behaviour of the specific materials we are considering. In our case an elasto-viscoplastic material is considered which is deformed due to the application of a direct electric current across the domain and the generation of heat in the part. Thus, the mechanical model involves electrical and thermal effects which must be computed by solving their respective models, which are also affected by the mechanical deformation.

Regarding the electrical model, it allows us to calculate the current density which causes the Joule effect and acts as a heat source in the thermal model. Since we are dealing with DC sources, the electrical model can be written in terms of the electric potential.

The boundary Γ_t for the electrical problem is decomposed into two disjoint parts, $\Gamma_t = \Gamma_t^{DE} \cup \Gamma_t^{NE}$, being the electric potential prescribed on Γ_t^{DE}, while the normal component of the current density is imposed on Γ_t^{NE}, $t \in [t_0, t_f]$ (see Fig. 5).

Thus, we consider the following boundary value problem to compute the electric potential.

Eulerian electrical problem (EEP). *Find an electric potential* $V : \mathcal{T} \longrightarrow \mathbb{R}$ *such that*

$$-\mathrm{div}(\check{\sigma}(\Theta)\mathrm{grad}V) = 0, \ \ in\ \mathcal{T}, \tag{22}$$

subject to the boundary conditions

$$V(\mathrm{x}, t) = V^D(\mathrm{x}, t), \quad \forall \mathrm{x} \in \Gamma_t^{DE}, \tag{23}$$

$$-\check{\sigma}(\Theta(\mathrm{x}, t))\mathrm{grad}V(\mathrm{x}, t) \cdot \mathbf{n}(\mathrm{x}, t) = g(\mathrm{x}, t), \quad \forall \mathrm{x} \in \Gamma_t^{NE}, \tag{24}$$

for $t \in [t_0, t_f]$.

In the above problem, $\check{\sigma} : \mathbb{R} \longrightarrow \mathbb{R}$ (electrical conductivity as function of temperature), $g(\cdot, t) : \Gamma_t^{NE} \longrightarrow \mathbb{R}$ (normal component of current density), $V^D(\cdot, t) : \Gamma_t^{DE} \longrightarrow \mathbb{R}$ (electric potential on Dirichlet boundary), $t \in [t_0, t_f]$, are given scalar fields, and $\Theta : \mathcal{T} \longrightarrow \mathbb{R}$ is the temperature (unknown) which is computed by solving the heat transfer problem below.

Note that the electrical conductivity and also the mechanical properties of the material are temperature-dependent. The temperature field is computed from the energy conservation equation, which includes the Joule effect as a heat source.

Let us decompose the boundary Γ_t for the thermal problem into two disjoint parts, $\Gamma_t = \Gamma_t^{DT} \cup \Gamma_t^{RT}$, and suppose the temperature is known on Γ_t^{DT}, while a convection-radiation boundary condition is imposed on Γ_t^{RT} (see Fig. 6). Finally, we suppose that temperature

is given at initial time. Thus, this evolution is governed by the following initial-boundary value problem derived from the energy balance equation.

Eulerian thermal problem (ETP). *Find a temperature field* $\Theta : \mathcal{T} \longrightarrow \mathbb{R}$ *such that*

$$\rho \check{c}_p(\Theta)\left(\frac{\partial \Theta}{\partial t} + \mathbf{v}\cdot \mathrm{grad}\Theta\right) - \mathrm{div}(\check{k}(\Theta)\mathrm{grad}\Theta) = \check{\sigma}(\Theta)|\mathrm{grad}V|^2, \ \ in\ \mathcal{T}, \tag{25}$$

subject to the boundary conditions

$$\Theta(\mathsf{x},t) = \Theta^D(\mathsf{x},t), \quad \forall \mathsf{x} \in \Gamma_t^{DT}, \tag{26}$$

$$\begin{aligned}\check{k}(\Theta(\mathsf{x},t))\mathrm{grad}\Theta(\mathsf{x},t)\cdot \mathbf{n}(\mathsf{x},t) &= h(\mathsf{x},t)(\Theta^C(\mathsf{x},t) - \Theta(\mathsf{x},t)) \\ &\quad + \sigma_{SB}\epsilon(\mathsf{x},t)((\Theta^R(\mathsf{x},t))^4 - \Theta^4(\mathsf{x},t)), \quad \forall \mathsf{x} \in \Gamma_t^{RT},\end{aligned} \tag{27}$$

for $t \in (t_0, t_f]$*, and the initial condition*

$$\Theta(\mathsf{x},t_0) = \Theta^0(\mathsf{x}), \quad \forall \mathsf{x} \in \overline{\Omega}_{t_0}. \tag{28}$$

In the above equations, $\check{c}_p : \mathbb{R} \longrightarrow \mathbb{R}$ (specific heat as function of temperature), $\check{k} : \mathbb{R} \longrightarrow \mathbb{R}$ (thermal conductivity as function of temperature), $\Theta^D(\cdot,t) : \Gamma_t^{DT} \longrightarrow \mathbb{R}$ (temperature on Dirichlet boundary), $h(\cdot,t) : \Gamma_t^{RT} \longrightarrow \mathbb{R}$ (heat transfer coefficient), $\epsilon(\cdot,t) : \Gamma_t^{RT} \longrightarrow \mathbb{R}$ (emissivity), $\Theta^C(\cdot,t) : \Gamma_t^{RT} \longrightarrow \mathbb{R}$ (convection temperature), $\Theta^R(\cdot,t) : \Gamma_t^{RT} \longrightarrow \mathbb{R}$ (radiation temperature), $\Theta^0 : \overline{\Omega} \longrightarrow \mathbb{R}$ (initial temperature), $t \in [t_0, t_f]$, are given scalar fields, and $\sigma_{SB} = 5.67 \times 10^{-8}\,\mathrm{Wm^{-2}K^{-4}}$ is the Stefan–Boltzmann constant.

As we advanced above, the thermal source term models the Joule effect that depends on the electric potential which is computed from the solution of the electrical problem. This term and the temperature dependence of the electrical conductivity couple the thermal and the electrical models, both of which are coupled, in turn, with the mechanical model by the motion.

We notice that equations appearing in the above thermo-electrical-mechanical model are expressed in spatial coordinates, $\mathsf{x} = \mathsf{X}(\mathsf{p},t)$, belonging, in general, to an unknown domain over time. In order to avoid this difficulty we will rewrite the above problems in the (time-independent) reference configuration $\overline{\Omega}$ which is supposed to be given.

In accordance with the weak formulation, scalar-valued Lebesgue and Sobolev spaces $L^2(\mathcal{A})$ and $H^1(\mathcal{A})$ will be used, where $\mathcal{A}$ denotes a bounded open set in $\mathbb{R}^d$. We denote by $H^1_{\Gamma^P}(\mathcal{A})$ the subspace of $H^1(\mathcal{A})$ defined by

$$H^1_{\Gamma^P}(\mathcal{A}) := \left\{ w \in H^1(\mathcal{A}) : \ w_{|\Gamma^P} = 0 \right\}, \tag{29}$$

where Γ^P is a subset of the boundary of $\mathcal{A}$ of non-null measure. Moreover, vector-valued function spaces will be distinguished using bold fonts, specifically $\mathbf{L}^2(\mathcal{A})$, $\mathbf{H}^1(\mathcal{A})$ and $\mathbf{H}^1_{\Gamma^P}(\mathcal{A})$. Similarly, tensor-valued function spaces will be denoted by $\mathbb{L}^2(\mathcal{A})$, $\mathbb{H}^1(\mathcal{A})$ and $\mathbb{H}^1_{\Gamma^P}(\mathcal{A})$.

4. Pure-Lagrangian approach: Strong problem and weak formulation

We are going to develop some formal computations in order to write the above coupled problems (**EGMP**), (**EEP**) and (**ETP**) in Lagrangian coordinates. First, the (general) Lagrangian motion equation is obtained and complemented with an elasto-viscoplastic constitutive model for large deformations. Then, we introduce the Lagrangian formulations of the thermal and electrical problems, noting that the electrical problem is a particular case of the thermal one.

4.1. Mechanical problem in Lagrangian coordinates

Firstly, we use the divergence theorem, the change of variable $\mathsf{x} = \mathsf{X}(\mathsf{p},t)$, the chain rule and the localization theorem, to obtain the equality

$$-\mathrm{div}_{\mathsf{x}}\mathbf{T}(\mathsf{x},t) = -\left\{ \mathrm{Div}_{\mathsf{p}}\left(\mathbf{T}_m(\mathsf{p},t)\det\mathbf{F}(\mathsf{p},t)\mathbf{F}^{-t}(\mathsf{p},t)\right)\frac{1}{\det\mathbf{F}(\mathsf{p},t)}\right\}\Bigg|_{\mathsf{p}=\mathsf{P}(\mathsf{x},t)}, \tag{30}$$

for $(\mathsf{x},t) \in \mathcal{T}$. Then, we evaluate Eqs. (15)–(20) at point $\mathsf{x} = \mathsf{X}(\mathsf{p},t)$ to obtain the following material versions of the boundary conditions:

$$\mathbf{u}(\mathsf{p},t) = \mathbf{u}^{\mathrm{D}}(\mathsf{p},t), \quad \forall (\mathsf{p},t) \in \Gamma^{DM} \times (t_0,t_f], \tag{31}$$

$$\mathbf{T}_m(\mathsf{p},t)\mathbf{F}^{-t}(\mathsf{p},t)\mathbf{m}(\mathsf{p}) = |\mathbf{F}^{-t}(\mathsf{p},t)\mathbf{m}(\mathsf{p})|\mathbf{h}_m(\mathsf{p},t), \quad \forall (\mathsf{p},t) \in \Gamma^{NM} \times (t_0,t_f], \tag{32}$$

$$\mathbf{T}_m(\mathsf{p},t)\mathbf{F}^{-t}(\mathsf{p},t)\mathbf{m}(\mathsf{p}) = -\tilde{\zeta}_m(\mathsf{p},t)\mathbf{F}^{-t}(\mathsf{p},t)\mathbf{m}(\mathsf{p}), \quad \forall (\mathsf{p},t) \in \Gamma^{CM} \times (t_0,t_f], \tag{33}$$

$$M(\mathsf{X}(\mathsf{p},t)) \geq 0, \quad \forall (\mathsf{p},t) \in \Gamma^{CM} \times (t_0,t_f], \tag{34}$$

$$\tilde{\zeta}_m(\mathsf{p},t) \geq 0, \quad \forall (\mathsf{p},t) \in \Gamma^{CM} \times (t_0,t_f], \tag{35}$$

$$\tilde{\zeta}_m(\mathsf{p},t)M(\mathsf{X}(\mathsf{p},t)) = 0, \quad \forall (\mathsf{p},t) \in \Gamma^{CM} \times (t_0,t_f], \tag{36}$$

being $\mathbf{m}$ the outward unit normal vector to Γ, and where

$$\mathbf{n}(\mathsf{X}(\mathsf{p},t),t) = \frac{\mathbf{F}^{-t}(\mathsf{p},t)\mathbf{m}(\mathsf{p})}{|\mathbf{F}^{-t}(\mathsf{p},t)\mathbf{m}(\mathsf{p})|}, \quad (\mathsf{p},t) \in \Gamma \times [t_0,t_f]. \tag{37}$$

The nonlinear complementarity problem (34)–(36) is reformulated by using a function ϕ_{NCP} satisfying the following properties (see [21] for details):

$$\phi_{NCP}(a,b) = 0 \Leftrightarrow a \geq 0, \quad b \geq 0, \quad a \cdot b = 0. \tag{38}$$

Then, the nonlinear complementarity problem (34)–(36) becomes

$$\phi_{NCP}(\tilde{\zeta}_m, M \circ \mathsf{X}) = 0, \quad \text{on } \Gamma^{CM} \times (t_0,t_f]. \tag{39}$$

As a consequence of these results and by evaluating equations of problem **(EGMP)** at point $\mathsf{x} = \mathsf{X}(\mathsf{p},t)$, we get the following formulation in $\overline{\Omega} \times [t_0,t_f]$:

Lagrangian general mechanical problem (LGMP). *Find three functions* $\mathbf{v}_m : \overline{\Omega} \times [t_0,t_f] \longrightarrow \mathbb{R}^d$, $\mathbf{T}_m : \overline{\Omega} \times [t_0,t_f] \longrightarrow Lin$ *and* $\tilde{\zeta}_m : \Gamma^{CM} \times [t_0,t_f] \to \mathbb{R}$ *satisfying*

$$\rho_m \dot{\mathbf{v}}_m - \frac{1}{\det \mathbf{F}} \mathrm{Div}_{\mathsf{p}} \left(\mathbf{T}_m \det \mathbf{F}\mathbf{F}^{-t} \right) = \mathbf{b}_m, \tag{40}$$

in $\Omega \times (t_0,t_f]$, *subjected to boundary conditions* (31)–(33) and (39), *and initial condition* (21).

In order to complete the above system, we are going to consider an elasto-viscoplasticity model which is defined by assuming a multiplicative decomposition; see [22] for a comprehensive explanation of this kind of decomposition at finite strains. More precisely, we assume the Kröner decomposition of the deformation gradient:

$$\mathbf{F} = \mathbf{F}^{\mathrm{e}}\mathbf{F}^{\mathrm{p}},$$

where $\mathbf{F}^{\mathrm{e}}$ and $\mathbf{F}^{\mathrm{p}}$ are called, respectively, the elastic and plastic deformation gradients. This multiplicative split of $\mathbf{F}$, introduced by Lee and Liu [23] and Lee [24], embodies the assumption of the existence of a local unstressed intermediate configuration defined by the plastic deformation gradient, $\mathbf{F}^{\mathrm{p}}$. However, it is generally not possible to find a motion X^{p} such that

$$\mathbf{F}^{\mathrm{p}} = \nabla \mathsf{X}^{\mathrm{p}}.$$

The deformation gradients $\mathbf{F}$, $\mathbf{F}^{\mathrm{p}}$ and $\mathbf{F}^{\mathrm{e}}$ have polar decompositions, more precisely,

$$\mathbf{F} = \mathbf{R}\mathbf{U} = \mathbf{V}\mathbf{R}, \quad \mathbf{F}^{\mathrm{p}} = \mathbf{R}^{\mathrm{p}}\mathbf{U}^{\mathrm{p}} = \mathbf{V}^{\mathrm{p}}\mathbf{R}^{\mathrm{p}}, \quad \mathbf{F}^{\mathrm{e}} = \mathbf{R}^{\mathrm{e}}\mathbf{U}^{\mathrm{e}} = \mathbf{V}^{\mathrm{e}}\mathbf{R}^{\mathrm{e}},$$

where $\mathbf{R}$, $\mathbf{R}^{\mathrm{p}}$ and $\mathbf{R}^{\mathrm{e}}$ are rotation tensor fields and $\mathbf{V}$, $\mathbf{U}$, $\mathbf{V}^{\mathrm{p}}$, $\mathbf{U}^{\mathrm{p}}$, $\mathbf{U}^{\mathrm{e}}$, $\mathbf{V}^{\mathrm{e}}$ are positive definite symmetric tensors. In order to model the elastic part, we use the Hencky strain energy by noting that only the elastic part of $\mathbf{F}$ produces stresses. The Hencky elasticity model is an isotropic finite elasticity model that successfully extends the infinitesimal framework to moderately large deformations, as those appearing in the considered problem. More precisely, the constitutive equation can be written in terms of the elastic left Hencky strain tensor as follows

$$\mathbf{K} = 2\breve{\mu}(\Theta)\mathbf{H}^{\mathrm{e}}_L + \breve{\lambda}(\Theta)\mathrm{tr}(\mathbf{H}^{\mathrm{e}}_L)\mathbf{I},$$

being $\breve{\lambda}(\Theta)$ and $\breve{\mu}(\Theta)$ the Lamé coefficients which are assumed to be temperature dependent, $\mathbf{K}$ the Kirchhoff stress tensor, and $\mathbf{H}^{\mathrm{e}}_{\mathbf{L}}$ the elastic left Hencky strain tensor, namely,

$$\mathbf{K} := \det \mathbf{F}^{\mathrm{e}}\mathbf{T}_m,$$
$$\mathbf{H}^{\mathrm{e}}_{\mathbf{L}} := \ln \mathbf{V}^{\mathrm{e}} = \frac{1}{2} \ln \left(\mathbf{F}^{\mathrm{e}}(\mathbf{F}^{\mathrm{e}})^t \right).$$

We note that this is a direct generalization of the classical Hooke's law for isotropic infinitesimal elasticity, by replacing the Cauchy stress tensor and the infinitesimal strain tensor by the Kirchhoff stress tensor and the left Hencky strain tensor, respectively.

In addition, a rate-dependent plasticity model must be used for the inelastic part of the material deformation. For this, we propose the Anand model which unifies creep and plasticity, and consists of two coupled differential equations that relate the inelastic strain rate to the rate of deformation resistance for materials with large, isotropic viscoplastic deformation but small elastic deformations. The Anand model was initially introduced to analyze the rate-dependent deformation of metals at high temperatures and is the most popular viscoplastic model in the framework of solder joint analysis (see, for instance, [25]). Among its specific features, we can mention that this model needs no explicit yield condition and no loading/unloading criterion, and that involves only one state variable which accurately and completely describes the constitutive behaviour of the mechanisms of plastic deformation in metals under physical and experimental considerations. More precisely, we assume that the plastic part is symmetric ($\mathbf{W}^{\mathrm{p}} = \mathbf{0}$), and that the spatially rotated plastic stretching can be written in terms of the deviatoric tensor of $\mathbf{K}$, to be denoted by $\mathbf{K}^{\mathrm{d}}$, as follows

$$\mathbf{R}^{\mathrm{e}}(\mathsf{p},t)\mathbf{D}^{\mathrm{p}}(\mathsf{p},t)(\mathbf{R}^{\mathrm{e}}(\mathsf{p},t))^t = \dot{\epsilon}^{\mathrm{p}}(\mathsf{p},t) \left(\frac{3}{2} \frac{\mathbf{K}^{\mathrm{d}}(\mathsf{p},t)}{q(\mathbf{K}^{\mathrm{d}}(\mathsf{p},t))} \right),$$

where $q(\mathbf{K}^{\mathrm{d}}) = \sqrt{\frac{3}{2}\mathbf{K}^{\mathrm{d}} : \mathbf{K}^{\mathrm{d}}}$. In order to compute the inelastic strain rate, $\dot{\epsilon}^{\mathrm{p}}(\mathrm{p}, t)$, a constitutive equation is given, namely,

$$\dot{\epsilon}^{\mathrm{p}}(\mathrm{p}, t) = A \exp\left(-\frac{Q}{R\,\Theta_m(\mathrm{p}, t)}\right)\left[\sinh\left(\xi \frac{q(\mathbf{K}^{\mathrm{d}}(\mathrm{p}, t))}{s(\mathrm{p}, t)}\right)\right]^{\frac{1}{m}}, \tag{41}$$

where A is the pre-exponential factor, Q is the activation energy, R is the universal gas constant, Θ is the temperature, ξ the stress multiplier, m is the strain rate sensitivity of stress, and s is a scalar internal variable, called deformation resistance, introduced to characterize *strain-hardening*. Moreover, in order to complete the constitutive equations for plastic flow, we assume that s evolves according to a differential equation, called *hardening equation*, of the form

$$\dot{s}(\mathrm{p}, t) = h(\dot{\epsilon}^{\mathrm{p}}(\mathrm{p}, t), s(\mathrm{p}, t), \Theta_m(\mathrm{p}, t)), \tag{42}$$

where

$$h(\dot{\epsilon}^{\mathrm{p}}, s, \Theta_m) = \left\{ h_0 \left| 1 - \frac{s}{s^*(\dot{\epsilon}^{\mathrm{p}}, \Theta_m)} \right|^a \operatorname{sign}\left(1 - \frac{s}{s^*(\dot{\epsilon}^{\mathrm{p}}, \Theta_m)}\right) \right\} \dot{\epsilon}^{\mathrm{p}}, \tag{43}$$

and s^* describes the saturation value of s associated with a coupled of given temperature and strain rate, namely,

$$s^*(\dot{\epsilon}^{\mathrm{p}}, \Theta_m) = \widetilde{s}\left[\frac{\dot{\epsilon}^{\mathrm{p}}}{A} \exp\left(\frac{Q}{R\,\Theta_m}\right)\right]^n. \tag{44}$$

In the above hardening equation, h_0 represents the hardening/softening constant, a is the strain rate sensitivity of hardening/softening, n stands for the strain rate sensitivity for the saturation value of the deformation resistance, and $\widetilde{s}$ is a coefficient related to the deformation resistance saturation. Finally, we have the following elasto-viscoplastic problem written in the reference configuration.

Lagrangian elasto-viscoplastic mechanical problem (LVMP). *Find four functions* $\mathbf{v}_m : \overline{\Omega} \times [t_0, t_f] \longrightarrow \mathbb{R}^d$, $\mathbf{F}^p : \overline{\Omega} \times [t_0, t_f] \longrightarrow Lin$, $s : \overline{\Omega} \times [t_0, t_f] \longrightarrow \mathbb{R}$ *and* $\tilde{\zeta}_m : \Gamma^{CM} \times [t_0, t_f] \to \mathbb{R}$ *satisfying*

$$\rho_0 \dot{\mathbf{v}}_m = \mathrm{Div}\left(\mathbf{K}\,(\mathbf{I} + \nabla\,\mathbf{u})^{-t}\right) + \det(\mathbf{I} + \nabla\,\mathbf{u})\,\mathbf{b}_m, \tag{45}$$

$$\dot{\mathbf{F}}^p\,(\mathbf{F}^p)^{-1} = \mathbf{R}^{e,t}\left(\frac{3}{2}\frac{\mathbf{K}^d}{q\,(\mathbf{K}^d)}\dot{\epsilon}^p\right)\mathbf{R}^e, \tag{46}$$

$$\dot{s} = \left\{ h_0 \left| 1 - \frac{s}{s^*} \right|^a \operatorname{sign}\left(1 - \frac{s}{s^*}\right) \right\} \dot{\epsilon}^p, \tag{47}$$

in $\Omega \times (t_0, t_f]$, *subjected to boundary conditions* (31)–(33) and (39), *and to initial conditions*

$$\mathbf{u}(\mathrm{p}, t_0) = \mathbf{u}^0(\mathrm{p}), \quad \forall \mathrm{p} \in \overline{\Omega}, \tag{48}$$

$$\mathbf{v}_m(\mathrm{p}, t_0) = \mathbf{v}_m^0(\mathrm{p}), \quad \forall \mathrm{p} \in \overline{\Omega}, \tag{49}$$

$$s(\mathrm{p}, t_0) = s^0(\mathrm{p}), \quad \forall \mathrm{p} \in \overline{\Omega}, \tag{50}$$

$$\mathbf{F}^p(\mathrm{p}, t_0) = \mathbf{I}, \quad \forall \mathrm{p} \in \overline{\Omega}, \tag{51}$$

being $\mathbf{u}^0 : \overline{\Omega} \longrightarrow \mathbb{R}^d$ *and* $s^0 : \overline{\Omega} \longrightarrow \mathbb{R}$ *two given fields, and where*

$$\mathbf{K} = 2\breve{\mu}(\Theta_m)\mathbf{H}_{\mathbf{L}}^e + \breve{\lambda}(\Theta_m)\mathrm{tr}\left(\mathbf{H}_{\mathbf{L}}^e\right)\mathbf{I}, \tag{52}$$

$$\mathbf{H}_{\mathbf{L}}^e = \frac{1}{2}\ln\left((\mathbf{I} + \nabla\,\mathbf{u})(\mathbf{F}^p)^{-1}(\mathbf{F}^p)^{-t}(\mathbf{I} + \nabla\,\mathbf{u})^t\right), \tag{53}$$

$$\mathbf{R}^e = \left[(\mathbf{I} + \nabla\,\mathbf{u})\,(\mathbf{F}^p)^{-1}\,(\mathbf{F}^p)^{-t}\,(\mathbf{I} + \nabla\,\mathbf{u})^t\right]^{-1/2}(\mathbf{I} + \nabla\,\mathbf{u})\,(\mathbf{F}^p)^{-1}, \tag{54}$$

$$\dot{\epsilon}^p = A \exp\left(-\frac{Q}{R\,\Theta_m}\right)\left[\sinh\left(\xi\frac{q(\mathbf{K}^d)}{s}\right)\right]^{\frac{1}{m}}, \tag{55}$$

$$s^* = \widetilde{s}\left[\frac{\dot{\epsilon}^p}{A}\exp\left(\frac{Q}{R\,\Theta_m}\right)\right]^n, \tag{56}$$

in $\overline{\Omega} \times (t_0, t_f]$.

Notice that in many cases the reference domain Ω is taken to be the initial configuration of the body and then the initial displacement is null.

Now, in order to write a weak formulation of the above problem **(LVMP)** we use function spaces $\mathbf{H}^1$ for the velocity/displacement, and L^2 tensor and scalar for $\mathbf{F}^p$ and s, respectively. Let us multiply (45) by $\mathbf{z} \in \mathbf{H}^1_{\Gamma^{DM}}(\Omega)$, integrate in Ω, and apply the usual Green's formula and boundary conditions (32), (33) and (39). Similarly, let us multiply (39), (46) and (47) by test functions belonging to L^2 spaces, and integrate in Ω. We get the following weak formulation for **(LVMP)**:

$$\int_\Omega \rho_0 \dot{\mathbf{v}}_m \cdot \mathbf{z}\,\mathrm{d}V_\mathsf{p} + \int_\Omega \left(\mathbf{K}\,\mathbf{F}^{-t}\right) : \nabla \mathbf{z}\,\mathrm{d}V_\mathsf{p} + \int_{\Gamma^{\mathsf{CM}}} \tilde{\zeta}_m \det \mathbf{F}\,\left(\mathbf{F}^{-t}\mathbf{m}\right)\cdot \mathbf{z}\,\mathrm{d}A_\mathsf{p}$$
$$= \int_{\Gamma^{\mathsf{NM}}} \det \mathbf{F}|\mathbf{F}^{-t}\mathbf{m}|\mathbf{h}_m \cdot \mathbf{z}\,\mathrm{d}A_\mathsf{p} + \int_\Omega \det \mathbf{F}\mathbf{b}_m \cdot \mathbf{z}\,\mathrm{d}V_\mathsf{p} \quad \forall \mathbf{z} \in \mathbf{H}^1_{\Gamma^{DM}}(\Omega),$$
$$\int_{\Gamma^{\mathsf{CM}}} \phi_{NCP}\left(\tilde{\zeta}_m, M\left(\mathsf{X}(\mathsf{p},t)\right)\right)\mu\,\mathrm{d}A_\mathsf{p} = 0 \quad \forall \mu \in L^2(\Gamma^{\mathsf{CM}}),$$
$$\int_\Omega \dot{\mathbf{F}}^p\left(\mathbf{F}^p\right)^{-1} : \mathbf{Q}\,\mathrm{d}V_\mathsf{p} = \int_\Omega \mathbf{R}^{e,t}\left(\frac{3}{2}\frac{\mathbf{K}^d}{q\left(\mathbf{K}^d\right)}\dot{e}^p\right)\mathbf{R}^e : \mathbf{Q}\,\mathrm{d}V_\mathsf{p} \quad \forall \mathbf{Q} \in \mathbb{L}^2(\Omega),$$
$$\int_\Omega \dot{s} w\,\mathrm{d}V_\mathsf{p} = \int_\Omega \left\{h_0\left|1-\frac{s}{s^*}\right|^a \mathrm{sign}\left(1-\frac{s}{s^*}\right)\right\}\dot{e}^p w\,\mathrm{d}V_\mathsf{p} \quad \forall w \in L^2(\Omega).$$

These are formal computations, i.e., we have assumed appropriate regularity of the involved fields.

Remark 4.1. In the particular case of surface loads of the form $\mathbf{h}(\mathsf{x},t) = -h(t)\mathbf{n}(\mathsf{x},t)$, the total resultant force $\mathbf{P}(t)$ can be written in Lagrangian coordinates as follows

$$\mathbf{P}(t) = \int_{\Gamma^{NM}} \mathbf{h}_m(t)\det \mathbf{F}(\mathsf{p},t)|\mathbf{F}^{-t}(\mathsf{p},t)\mathbf{m}(\mathsf{p})|\,\mathrm{d}A_\mathsf{p}.$$

If the known data is $\mathbf{P}(t)$, this equation relating $\mathbf{P}(t)$ and $\mathbf{h}_m(t)$ must be added to the system.

4.2. Thermal problem in Lagrangian coordinates

We are going to develop formal computations analogous to the ones in the previous section but in the scalar case, in order to write a weak formulation of the above thermal problem (**ETP**) in Lagrangian configuration.

First, by evaluating Eq. (25) at point $\mathsf{x} = \mathsf{X}(\mathsf{p},t)$ and then using (7) and (9) for $\Psi = \Theta$ and $\Psi = \Theta,\ V$, respectively, we obtain

$$\rho_m \check{c}_p(\Theta_m)\dot{\Theta}_m - \mathrm{div}_\mathsf{x}(\check{k}(\Theta_m)\mathbf{F}^{-t}\nabla_\mathsf{p}\Theta_m) = \check{\sigma}(\Theta_m)|\mathbf{F}^{-t}\nabla_\mathsf{p}V_m|^2, \quad \text{in } \Omega\times(t_0,t_f]. \tag{57}$$

Notice that in (57) there are derivatives with respect to the Eulerian variable x. In order to obtain a strong formulation of problem (**ETP**) in Lagrangian coordinates we use the divergence theorem, the change of variable $\mathsf{x} = \mathsf{X}(\mathsf{p},t)$ and the localization theorem to get

$$\mathrm{div}_\mathsf{x}(\check{k}(\Theta_m(\mathsf{p},t))\mathbf{F}^{-t}(\mathsf{p},t)\nabla_\mathsf{p}\Theta_m(\mathsf{p},t))$$
$$= \mathrm{Div}_\mathsf{p}\left[\check{k}(\Theta_m(\mathsf{p},t))\mathbf{F}^{-1}(\mathsf{p},t)\mathbf{F}^{-t}(\mathsf{p},t)\nabla_\mathsf{p}\Theta_m(\mathsf{p},t)\det\mathbf{F}(\mathsf{p},t)\right]\left.\frac{1}{\det\mathbf{F}(\mathsf{p},t)}\right|_{\mathsf{p}=\mathsf{P}(\mathsf{x},t)}, \tag{58}$$

for $(\mathsf{x},t)\in\mathcal{T}$. Moreover, from (26) and (27), we obtain the following boundary conditions for Θ_m:

$$\Theta_m(\mathsf{p},t) = \Theta_m^D(\mathsf{p},t), \quad \forall(\mathsf{p},t)\in\Gamma^{DT}\times(t_0,t_f], \tag{59}$$
$$\check{k}(\Theta_m(\mathsf{p},t))\mathbf{F}^{-t}(\mathsf{p},t)\nabla\Theta_m(\mathsf{p},t)\cdot\frac{\mathbf{F}^{-t}(\mathsf{p},t)\mathbf{m}(\mathsf{p})}{|\mathbf{F}^{-t}(\mathsf{p},t)\mathbf{m}(\mathsf{p})|}$$
$$= h_m(\mathsf{p},t)(\Theta_m^C(\mathsf{p},t)-\Theta_m(\mathsf{p},t)) + \sigma_{SB}\epsilon_m(\mathsf{p},t)((\Theta_m^R(\mathsf{p},t))^4 - \Theta_m^4(\mathsf{p},t)), \quad \forall(\mathsf{p},t)\in\Gamma^{RT}\times(t_0,t_f], \tag{60}$$

The second condition has been obtained by using the chain rule and (37). Thus, we have the following formulation in $\Omega\times[t_0,t_f]$ of the initial-boundary value problem (**ETP**):

Lagrangian thermal problem (LTP). *Find a temperature field* $\Theta_m : \overline{\Omega}\times[t_0,t_f] \longrightarrow \mathbb{R}$ *such that*

$$\rho_0\check{c}_p(\Theta_m)\dot{\Theta}_m - \mathrm{Div}\left[\check{k}(\Theta_m)\mathbf{F}^{-1}\mathbf{F}^{-t}\nabla\Theta_m\det\mathbf{F}\right] = \det\mathbf{F}\check{\sigma}(\Theta_m)|\mathbf{F}^{-t}\nabla V_m|^2, \tag{61}$$

in $\Omega\times(t_0,t_f]$, *subjected to boundary conditions* (59) *and* (60), *and to initial condition* (28).

Next, we introduce the standard weak formulation associated with this pure-Lagrangian strong problem:

$$\int_\Omega \rho_0\check{c}_p(\Theta_m)\dot{\Theta}_m\psi\det\mathbf{F}\,\mathrm{d}V_\mathsf{p} + \int_\Omega \check{k}(\Theta_m)\mathbf{F}^{-1}\mathbf{F}^{-t}\nabla\Theta_m\cdot\nabla\psi\det\mathbf{F}\,\mathrm{d}V_\mathsf{p}$$
$$-\int_{\Gamma^{RT}}\left[h_m(\Theta_m^C-\Theta_m)+\sigma_{SB}\epsilon_m((\Theta_m^R)^4-\Theta_m^4)\right]\psi\left|\mathbf{F}^{-t}\mathbf{m}\right|\det\mathbf{F}\,\mathrm{d}A_\mathsf{p}$$
$$= \int_\Omega \check{\sigma}(\Theta_m)|\mathbf{F}^{-t}\nabla V_m|^2\psi\det\mathbf{F}\,\mathrm{d}V_\mathsf{p},$$

$\forall\psi\in H^1_{\Gamma^{DT}}(\Omega)$ and $\forall t\in(t_0,t_f]$.

4.3. Electrical problem in Lagrangian coordinates

In order to write the considered Eulerian electrical problem, (**EEP**), in the reference configuration Ω, we apply the same procedures as in the previous section for this particular case. More precisely, we obtain the following strong formulation in $\Omega\times[t_0,t_f]$:

Lagrangian electrical problem (LEP). *Find an electric potential* $V_m : \overline{\Omega}\times[t_0,t_f]\longrightarrow\mathbb{R}$ *such that*

$$\mathrm{Div}\left[\det\mathbf{F}\mathbf{F}^{-1}\breve{\sigma}(\Theta_m)\mathbf{F}^{-t}\nabla V_m\right]=0, \tag{62}$$

in $\Omega\times[t_0,t_f]$, *subject to boundary conditions*

$$V_m = V_m^D, \quad on \quad \Gamma^{DE}\times[t_0,t_f], \tag{63}$$

$$-\breve{\sigma}(\Theta_m)\mathbf{F}^{-t}\nabla V_m\cdot\mathbf{F}^{-t}\mathbf{m} = |\mathbf{F}^{-t}\mathbf{m}|g_m, \quad on \quad \Gamma^{NE}\times[t_0,t_f]. \tag{64}$$

The standard weak formulation of **(LEP)** reads as follows:

$$\int_\Omega \breve{\sigma}(\Theta_m)\mathbf{F}^{-1}\mathbf{F}^{-t}\nabla V_m\cdot\nabla W\det\mathbf{F}\mathrm{d}V_{\mathsf{p}}+\int_{\Gamma^{NE}}|\mathbf{F}^{-t}\mathbf{m}|g_m\det\mathbf{F}W\mathrm{d}A_{\mathsf{p}}=0,\quad \forall W\in H^1_{\Gamma^{DE}}(\Omega). \tag{65}$$

5. Lagrangian weak formulation with cylindrical symmetry

In some situations, real forming devices can be approximated as being axisymmetric. This is the case for many electric upsetting processes, such as the in-die upsetting of a steel bar shown in Section 7. In the present section, we consider a three-dimensional case with cylindrical symmetry. More precisely, we assume that the reference domain $\Omega\subset\mathbb{R}^3$ can be obtained by rotating a bounded domain $\widehat{\Omega}\subset\mathbb{R}^2$, with boundary $\partial\widehat{\Omega}=\widehat{\Gamma}_{\mathrm{D}}\cup\widehat{\Gamma}$, around the axis of symmetry, $r_m=0$. That is,

$$\Omega := \{(r_m,\Theta_m,z_m) : \Theta_m\in[0,2\pi),(r_m,z_m)\in\widehat{\Omega}\}, \tag{66}$$

and

$$\Gamma := \partial\Omega = \{(r_m,\Theta_m,z_m) : \Theta_m\in[0,2\pi),(r_m,z_m)\in\widehat{\Gamma}\}. \tag{67}$$

Notice that $\widehat{\Gamma}_{\mathrm{D}}$ is defined by

$$\widehat{\Gamma}_{\mathrm{D}} := \{(r_m,z_m)\in\partial\widehat{\Omega} : r_m=0\}. \tag{68}$$

Moreover, boundaries Γ^{DM}, Γ^{NM}, Γ^{CM}, Γ^{DT}, Γ^{RT}, Γ^{DE}, Γ^{NE} are obtained by rotating their corresponding parts of $\widehat{\Gamma}$ around the axis of symmetry. These parts are denoted by $\widehat{\Gamma}^{DM}$, $\widehat{\Gamma}^{NM}$, $\widehat{\Gamma}^{CM}$, $\widehat{\Gamma}^{DT}$, $\widehat{\Gamma}^{RT}$, $\widehat{\Gamma}^{DE}$, $\widehat{\Gamma}^{NE}$, respectively.

Finally, we assume that all of the fields appearing in the problem present cylindrical symmetry. They will be specified with a hat. More precisely, if ϕ_m is a scalar material field independent of the azimuthal coordinate, $\widehat{\phi}_m$ denotes its description related to $\widehat{\Omega}$, namely,

$$\phi_m(\mathsf{p},t) := \widehat{\phi}_m(\hat{\mathsf{p}},t), \tag{69}$$

where $\hat{\mathsf{p}} := (r_m,z_m)\in\widehat{\Omega}$ denotes radial and axial coordinates of the material point $\mathsf{p}\in\Omega$. Notice that a vector material field with cylindrical symmetry $\boldsymbol{\vartheta}_m$ is defined by their coordinates in the basis $\{\mathbf{e}_r,\mathbf{e}_\Theta,\mathbf{e}_z\}$ as follows

$$\boldsymbol{\vartheta}_m(\mathsf{p},t) := \widehat{\vartheta}_r(\hat{\mathsf{p}},t)\mathbf{e}_r+\widehat{\vartheta}_z(\hat{\mathsf{p}},t)\mathbf{e}_z, \tag{70}$$

being its coordinate vector denoted with a hat, namely,

$$\widehat{\boldsymbol{\vartheta}}_m(\hat{\mathsf{p}},t) := \begin{pmatrix}\widehat{\vartheta}_r(\hat{\mathsf{p}},t)\\ \widehat{\vartheta}_z(\hat{\mathsf{p}},t)\end{pmatrix}. \tag{71}$$

Let $\boldsymbol{\Psi}_m$ be a tensor material field with cylindrical symmetry. This means that its components do not explicitly depend on Θ and that they remain unchanged under a rotation about z. The most general form of such a tensor is

$$\begin{aligned}\boldsymbol{\Psi}_m(\mathsf{p},t) :=& \widehat{\Psi}_{rr}(\hat{\mathsf{p}},t)\mathbf{e}_r\otimes\mathbf{e}_r+\widehat{\Psi}_{rz}(\hat{\mathsf{p}},t)\mathbf{e}_r\otimes\mathbf{e}_z+\widehat{\Psi}_{\Theta\Theta}(\hat{\mathsf{p}},t)\mathbf{e}_\Theta\otimes\mathbf{e}_\Theta\\ &+\widehat{\Psi}_{zr}(\hat{\mathsf{p}},t)\mathbf{e}_z\otimes\mathbf{e}_r+\widehat{\Psi}_{zz}(\hat{\mathsf{p}},t)\mathbf{e}_z\otimes\mathbf{e}_z,\end{aligned} \tag{72}$$

for $\hat{\mathsf{p}} := (r_m,z_m)\in\widehat{\Omega}$. Moreover, let us introduce the material tensor field $\widehat{\boldsymbol{\Psi}}_m(\hat{\mathsf{p}},t)$ defined by their coordinates in the basis $\{\hat{\mathbf{e}}_r,\hat{\mathbf{e}}_z\}$ as

$$\widehat{\boldsymbol{\Psi}}_m(\hat{\mathsf{p}},t) := \begin{pmatrix}\widehat{\Psi}_{rr}(\hat{\mathsf{p}},t) & \widehat{\Psi}_{rz}(\hat{\mathsf{p}},t)\\ \widehat{\Psi}_{zr}(\hat{\mathsf{p}},t) & \widehat{\Psi}_{zz}(\hat{\mathsf{p}},t)\end{pmatrix}, \tag{73}$$

for $\widehat{\mathrm{p}} := (r_m, z_m) \in \widehat{\Omega}$. Differential operators applied to fields defined in $\widehat{\Omega}$ will be also denoted with a hat. More precisely,

$$\widehat{\nabla}\,\widehat{\phi}_m(\widehat{\mathrm{p}},t) = \begin{pmatrix} \dfrac{\partial\widehat{\phi}_m(\widehat{\mathrm{p}},t)}{\partial r_m} \\ \dfrac{\partial\widehat{\phi}_m(\widehat{\mathrm{p}},t)}{\partial z_m} \end{pmatrix}, \quad \widehat{\nabla}\,\widehat{\boldsymbol{\vartheta}}_m(\widehat{\mathrm{p}},t) = \begin{pmatrix} \dfrac{\partial\widehat{\vartheta}_r(\widehat{\mathrm{p}},t)}{\partial r_m} & \dfrac{\partial\widehat{\vartheta}_r(\widehat{\mathrm{p}},t)}{\partial z_m} \\ \dfrac{\partial\widehat{\vartheta}_z(\widehat{\mathrm{p}},t)}{\partial r_m} & \dfrac{\partial\widehat{\vartheta}_z(\widehat{\mathrm{p}},t)}{\partial z_m} \end{pmatrix}. \tag{74}$$

We note that, in the axisymmetric framework, the deformation gradient tensor $\mathbf{F}(\mathrm{p},t)$ has the form

$$\mathbf{F}(\mathrm{p},t) = \mathbf{I_3} + \nabla\,\mathbf{u}(\mathrm{p},t) = \begin{pmatrix} 1+\dfrac{\partial\widehat{u}_r(\widehat{\mathrm{p}},t)}{\partial r_m} & 0 & \dfrac{\partial\widehat{u}_r(\widehat{\mathrm{p}},t)}{\partial z_m} \\ 0 & 1+\dfrac{\widehat{u}_r(\widehat{\mathrm{p}},t)}{r_m} & 0 \\ \dfrac{\partial\widehat{u}_z(\widehat{\mathrm{p}},t)}{\partial r_m} & 0 & 1+\dfrac{\partial\widehat{u}_z(\widehat{\mathrm{p}},t)}{\partial z_m} \end{pmatrix}.$$

Moreover, with the above notation, we have

$$\widehat{\mathbf{F}}(\widehat{\mathrm{p}},t) = \mathbf{I_2} + \widehat{\nabla}\,\widehat{\mathbf{u}}(\widehat{\mathrm{p}},t) = \begin{pmatrix} 1+\dfrac{\partial\widehat{u}_r(\widehat{\mathrm{p}},t)}{\partial r_m} & \dfrac{\partial\widehat{u}_r(\widehat{\mathrm{p}},t)}{\partial z_m} \\ \dfrac{\partial\widehat{u}_z(\widehat{\mathrm{p}},t)}{\partial r_m} & 1+\dfrac{\partial\widehat{u}_z(\widehat{\mathrm{p}},t)}{\partial z_m} \end{pmatrix}, \tag{75}$$

$$\det\mathbf{F}(\mathrm{p},t) = \left(1+\frac{\widehat{u}_r(\widehat{\mathrm{p}},t)}{r_m}\right)\det\widehat{\mathbf{F}}(\widehat{\mathrm{p}},t). \tag{76}$$

In the axisymmetric framework, the Lagrangian thermo-electrical-mechanical weak problem can be defined in the meridional section $\widehat{\Omega}$ as follows.

Lagrangian elasto-viscoplastic weak mechanical problem with cylindrical symmetry. *Find four functions* $\widehat{\mathbf{v}}_m : \overline{\widehat{\Omega}}\times[t_0,t_f] \longrightarrow \mathbb{R}^2$, $\mathbf{F}^p : \overline{\widehat{\Omega}}\times[t_0,t_f] \longrightarrow Lin$, $\widehat{s} : \overline{\widehat{\Omega}}\times[t_0,t_f] \longrightarrow \mathbb{R}$, *and* $\widehat{\zeta}_m : \widehat{\Gamma}^{\mathrm{CM}}\times[t_0,t_f] \longrightarrow \mathbb{R}$ *satisfying*

$$\int_{\widehat{\Omega}} \widehat{\rho}_0\dot{\widehat{\mathbf{v}}}_m\cdot\widehat{\mathbf{z}}\,r_m\,\mathrm{d}r_m\mathrm{d}z_m + \int_{\widehat{\Omega}}\left(\widehat{\mathbf{K}}\,\widehat{\mathbf{F}}^{-t}\right) : \widehat{\nabla}\,\widehat{\mathbf{z}}\,r_m\,\mathrm{d}r_m\mathrm{d}z_m + \int_{\widehat{\Omega}}\frac{\widehat{K}_{\Theta\Theta}\widehat{z}_r}{r_m+\widehat{u}_r}r_m\,\mathrm{d}r_m\mathrm{d}z_m$$

$$\int_{\widehat{\Gamma}^{\mathrm{CM}}}\widehat{\zeta}_m\left(1+\frac{\widehat{u}_r}{r_m}\right)\det\widehat{\mathbf{F}}\left(\widehat{\mathbf{F}}^{-t}\widehat{\mathbf{m}}\right)\cdot\widehat{\mathbf{z}}\,r_m\,\mathrm{d}\widehat{l}_p = \int_{\widehat{\Gamma}^{\mathrm{NM}}}\left(1+\frac{\widehat{u}_r}{r_m}\right)\det\widehat{\mathbf{F}}|\widehat{\mathbf{F}}^{-t}\widehat{\mathbf{m}}|\widehat{\mathbf{h}}_m\cdot\widehat{\mathbf{z}}\,r_m\,\mathrm{d}\widehat{l}_p$$
$$+\int_{\widehat{\Omega}}\left(1+\frac{\widehat{u}_r}{r_m}\right)\det\widehat{\mathbf{F}}\,\widehat{\mathbf{b}}_m\cdot\widehat{\mathbf{z}}\,r_m\,\mathrm{d}r_m\mathrm{d}z_m,$$

$$\int_{\widehat{\Gamma}^{\mathrm{CM}}}\widehat{\phi}_{NCP}\left(\widehat{\zeta}_m,\widehat{M}\left(\widehat{\mathrm{X}}(\widehat{\mathrm{p}},t)\right)\right)\widehat{\mu}\,r_m\,\mathrm{d}\widehat{l}_p = 0,$$

$$\int_{\widehat{\Omega}}\dot{\mathbf{F}}^p(\mathbf{F}^p)^{-1} : \mathbf{Q}\,r_m\,\mathrm{d}r_m\mathrm{d}z_m = \int_{\widehat{\Omega}}\mathbf{R}^{e,t}\left(\frac{3}{2}\frac{\mathbf{K}^d}{q\left(\mathbf{K}^d\right)}\dot{\widehat{\epsilon}}^p\right)\mathbf{R}^e : \mathbf{Q}\,r_m\,\mathrm{d}r_m\mathrm{d}z_m,$$

$$\int_{\widehat{\Omega}}\dot{\widehat{s}}\widehat{w}\,r_m\,\mathrm{d}r_m\mathrm{d}z_m = \int_{\widehat{\Omega}}\left\{h_0\left|1-\frac{\widehat{s}}{\widehat{s}^*}\right|^a\mathrm{sign}\left(1-\frac{\widehat{s}}{\widehat{s}^*}\right)\right\}\dot{\widehat{\epsilon}}^p\widehat{w}\,r_m\,\mathrm{d}r_m\mathrm{d}z_m,$$

subject to the Dirichlet boundary and initial conditions

$$\widehat{\mathbf{u}}(\widehat{\mathrm{p}},t) = \widehat{\mathbf{u}}^{\mathrm{D}}(\widehat{\mathrm{p}},t), \quad \forall\widehat{\mathrm{p}}\in\widehat{\Gamma}^{DM}, \tag{77}$$

$$\widehat{u}_r(\widehat{\mathrm{p}},t) = 0, \quad \forall\widehat{\mathrm{p}}\in\widehat{\Gamma}_{\mathrm{D}}, \tag{78}$$

$$\widehat{\mathbf{u}}(\widehat{\mathrm{p}},t_0) = \widehat{\mathbf{u}}^0(\widehat{\mathrm{p}}), \quad \forall\widehat{\mathrm{p}}\in\overline{\widehat{\Omega}}, \tag{79}$$

$$\widehat{\mathbf{v}}_m(\widehat{\mathrm{p}},t_0) = \widehat{\mathbf{v}}_m^0(\widehat{\mathrm{p}}), \quad \forall\widehat{\mathrm{p}}\in\overline{\widehat{\Omega}}, \tag{80}$$

$$\widehat{s}(\widehat{\mathrm{p}},t_0) = \widehat{s}^0(\widehat{\mathrm{p}}), \quad \forall\widehat{\mathrm{p}}\in\overline{\widehat{\Omega}}, \tag{81}$$

$$\mathbf{F}^p(\widehat{\mathrm{p}},t_0) = \mathbf{I}, \quad \forall\widehat{\mathrm{p}}\in\overline{\widehat{\Omega}}, \tag{82}$$

for $t\in[t_0,t_f]$, *and where*

$$\mathbf{K} = 2\breve{\mu}(\widehat{\Theta}_m)\mathbf{H}_{\mathbf{L}}^e + \breve{\lambda}(\widehat{\Theta}_m)\mathrm{tr}\left(\mathbf{H}_{\mathbf{L}}^e\right)\mathbf{I}, \tag{83}$$

$$\mathbf{H}_{\mathbf{L}}^e = \frac{1}{2}\ln\left(\mathbf{F}\left(\mathbf{F}^p\right)^{-1}\left(\mathbf{F}^p\right)^{-t}\mathbf{F}^t\right), \tag{84}$$

$$\mathbf{R}^e = \left[\mathbf{F}\left(\mathbf{F}^p\right)^{-1}\left(\mathbf{F}^p\right)^{-t}\mathbf{F}^t\right]^{-1/2}\mathbf{F}\left(\mathbf{F}^p\right)^{-1}, \tag{85}$$

$$\dot{\widehat{\epsilon}}^p = A\exp\left(-\frac{Q}{R\widehat{\Theta}_m}\right)\left[\sinh\left(\xi\frac{q(\mathbf{K}^d)}{\widehat{s}}\right)\right]^{\frac{1}{m}}, \tag{86}$$

$$\widehat{s}^{*} = \widetilde{s}\left[\frac{\hat{\epsilon^{p}}}{A}\exp\left(\frac{Q}{R\widehat{\Theta}_{m}}\right)\right]^{n}, \tag{87}$$

in $\overline{\widehat{\Omega}}\times[t_0,t_f]$.

Lagrangian weak thermal problem with cylindrical symmetry. *Find a scalar field* $\widehat{\Theta}_m : \overline{\widehat{\Omega}}\times[t_0,t_f]\longrightarrow\mathbb{R}$ *such that*

$$\begin{aligned}
&\int_{\widehat{\Omega}}\widehat{\rho}_0\check{c}_p(\widehat{\Theta}_m)\dot{\widehat{\Theta}}_m\widehat{\psi}\,r_m\mathrm{d}r_m\mathrm{d}z_m+\int_{\widehat{\Omega}}\check{k}(\widehat{\Theta}_m)\widehat{\mathbf{F}}^{-1}\widehat{\mathbf{F}}^{-t}\widehat{\nabla}\widehat{\Theta}_m\cdot\widehat{\nabla}\widehat{\psi}\det\widehat{\mathbf{F}}\left(1+\frac{1}{r_m}\widehat{u}_r\right)r_m\mathrm{d}r_m\mathrm{d}z_m\\
&-\int_{\widehat{\Gamma}^{RT}}\left|\widehat{\mathbf{F}}^{-t}\widehat{\mathbf{m}}\right|\left[\widehat{h}_m\left(\widehat{\Theta}_m^{C}-\widehat{\Theta}_m\right)+\widehat{\epsilon}_m\sigma_{SB}\left((\widehat{\Theta}_m^{R})^4-\widehat{\Theta}_m^4\right)\right]\widehat{\psi}\det\widehat{\mathbf{F}}\left(1+\frac{1}{r_m}\widehat{u}_r\right)r_m\mathrm{d}\widehat{l}_{\mathrm{p}}\\
&=\int_{\widehat{\Omega}}\check{\sigma}(\widehat{\Theta}_m)\left|\widehat{\mathbf{F}}^{-t}\widehat{\nabla}\widehat{V}_m\right|^2\widehat{\psi}\det\widehat{\mathbf{F}}\left(1+\frac{1}{r_m}\widehat{u}_r\right)r_m\mathrm{d}r_m\mathrm{d}z_m,
\end{aligned}\tag{88}$$

subject to the Dirichlet boundary condition

$$\widehat{\Theta}_m(\widehat{\mathrm{p}},t)=\widehat{\Theta}^{DT}(\widehat{\mathrm{p}},t),\quad\forall\widehat{\mathrm{p}}\in\widehat{\Gamma}^{DT}, \tag{89}$$

for $t\in(t_0,t_f]$, *and to the initial condition*

$$\widehat{\Theta}_m(\widehat{\mathrm{p}},t_0)=\widehat{\Theta}_m^{0}(\widehat{\mathrm{p}}),\quad\forall\widehat{\mathrm{p}}\in\overline{\widehat{\Omega}}. \tag{90}$$

Lagrangian weak electrical problem with cylindrical symmetry. *Find an electric potential* $\widehat{V}_m : \overline{\widehat{\Omega}}\times[t_0,t_f]\longrightarrow\mathbb{R}$ *such that*

$$\begin{aligned}
&\int_{\widehat{\Omega}}\check{\sigma}(\widehat{\Theta}_m)\widehat{\mathbf{F}}^{-1}\widehat{\mathbf{F}}^{-t}\widehat{\nabla}\widehat{V}_m\cdot\widehat{\nabla}\widehat{W}\det\widehat{\mathbf{F}}\left(1+\frac{1}{r_m}\widehat{u}_r\right)r_m\mathrm{d}r_m\mathrm{d}z_m\\
&+\int_{\widehat{\Gamma}^{NE}}\left|\widehat{\mathbf{F}}^{-t}\widehat{\mathbf{m}}\right|\widehat{g}_m\widehat{W}\det\widehat{\mathbf{F}}\left(1+\frac{1}{r_m}\widehat{u}_r\right)r_m\mathrm{d}\widehat{l}_{\mathrm{p}}=0,
\end{aligned}\tag{91}$$

subject to the Dirichlet boundary condition

$$\widehat{V}_m(\widehat{\mathrm{p}},t)=\widehat{V}_m^{DE}(\widehat{\mathrm{p}},t),\quad\forall(\widehat{\mathrm{p}},t)\in\widehat{\Gamma}^{DE}\times[t_0,t_f]. \tag{92}$$

6. Time and space discretization

We propose a space discretization of the thermo-electrical-mechanical Lagrangian problem by using finite element spaces. For this, we suppose a bounded domain with Lipschitz polygonal boundary and consider a suitable family of regular triangulations compatible with the partitions of the boundary, consisting of elements K of diameter $\leq h$. The space semi-discretized problem constitutes a system of differential–algebraic equations (DAEs) that is solved by using Runge–Kutta schemes. We consider a quite general semi-discretized problem to introduce the fully discretized scheme. More precisely,

$$\widetilde{\mathbf{M}}(\widehat{\mathbf{y}}_d,\widehat{\mathbf{y}}_a)\dot{\widehat{\mathbf{y}}}_d=\widetilde{\mathbf{f}}(\widehat{\mathbf{y}}_d,\widehat{\mathbf{y}}_a,t), \tag{93a}$$

$$0=\widetilde{\mathbf{g}}(\widehat{\mathbf{y}}_d,\widehat{\mathbf{y}}_a), \tag{93b}$$

$$\widehat{\mathbf{y}}_d(\cdot,t)=\overline{\mathbf{y}}_d(\cdot,t),\ \text{on}\ \widehat{\Gamma}^{D}, \tag{93c}$$

$$\widehat{\mathbf{y}}_a(\cdot,t)=\overline{\mathbf{y}}_a(\cdot,t),\ \text{on}\ \widehat{\Gamma}^{D}, \tag{93d}$$

$$\widehat{\mathbf{y}}_d(\cdot,t_0)=\mathbf{y}_d^{0},\ \text{in}\ \overline{\widehat{\Omega}}, \tag{93e}$$

where $\widetilde{\mathbf{M}}$ is a non-singular matrix representing the mass matrix.

We use the following notation:

$$\widehat{\mathbf{y}}=\begin{bmatrix}\widehat{\mathbf{y}}_d\\ \widehat{\mathbf{y}}_a\end{bmatrix},\quad\overline{\mathbf{y}}=\begin{bmatrix}\overline{\mathbf{y}}_d\\ \overline{\mathbf{y}}_a\end{bmatrix},\quad\mathbf{f}=\begin{bmatrix}\widetilde{\mathbf{f}}\\ \widetilde{\mathbf{g}}\end{bmatrix},\quad\mathbf{M}=\begin{bmatrix}\widetilde{\mathbf{M}}&0\\ 0&0\end{bmatrix}, \tag{94}$$

to write the problem in a more compact form, namely,

$$\mathbf{M}(\widehat{\mathbf{y}})\dot{\widehat{\mathbf{y}}}=\mathbf{f}(\widehat{\mathbf{y}},t), \tag{95a}$$

$$\widehat{\mathbf{y}}(\cdot,t)=\overline{\mathbf{y}}(\cdot,t),\ \text{on}\ \widehat{\Gamma}^{D}, \tag{95b}$$

$$\widehat{\mathbf{y}}_d(\cdot,t_0)=\mathbf{y}_d^{0},\ \text{in}\ \overline{\widehat{\Omega}}. \tag{95c}$$

In order to solve these coupled problems, an implicit Runge–Kutta method defined in the PETSc framework will be used. The PETSc library [26–28] includes a temporal integration module called *time stepping ode solver* [29] allowing for the numerical resolution of ODEs and DAEs by means of different numerical schemes (Runge–Kutta, Rosenbrock–Wanner, BDF).

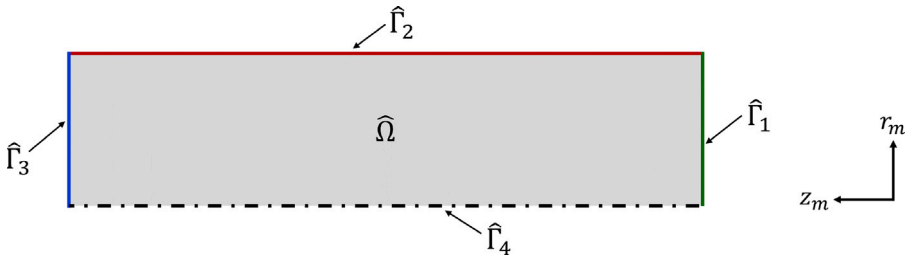

Fig. 7. Computational domain for Examples 1, 2 and 3.

For the resolution of the type problem stated in (95), the family of schemes called *ARKIMEX* is used, consisting of Runge–Kutta additive methods where it is possible to separate the problem into two parts, one treated implicitly and the other one explicitly. In the case of DAEs, only the implicit strategy involving the use of DIRK methods (Diagonal Implicit Runge–Kutta) is used.

Specifically, in problem (95), at each time instant t_n, $\hat{\mathbf{y}}^{n-1} \approx \hat{\mathbf{y}}(\cdot, t_{n-1})$ and the following system of nonlinear equations is solved for each stage $i \in [1, s]$ of the method:

$$\check{\mathbf{f}}(\mathbf{Y}_{n,i}, \dot{\mathbf{Y}}_{n,i}, t_{n-1} + c_i \Delta t) = \mathbf{M}(\mathbf{Y}_{n,i})\dot{\mathbf{Y}}_{n,i} - \mathbf{f}(\mathbf{Y}_{n,i}, t_{n-1} + c_i \Delta t) = 0, \tag{96a}$$

$$\mathbf{Z} = \hat{\mathbf{y}}^{n-1} + \Delta t \sum_{j=1}^{i-1} a_{ij} \dot{\mathbf{Y}}_{n,j}, \tag{96b}$$

$$\dot{\mathbf{Y}}_{n,i} = \frac{1}{\Delta t}(\mathbf{Y}_{n,i} - \mathbf{Z}), \tag{96c}$$

whose Jacobian matrix can be obtained by applying the chain rule and using (96c):

$$\begin{aligned} \frac{\mathrm{d}}{\mathrm{d}\mathbf{Y}_{n,i}}(\check{\mathbf{f}}(\mathbf{Y}_{n,i}, \dot{\mathbf{Y}}_{n,i}(\mathbf{Y}_{n,i}), \cdot)) &= \frac{\partial \check{\mathbf{f}}}{\partial \dot{\mathbf{Y}}_{n,i}}(\mathbf{Y}_{n,i}, \dot{\mathbf{Y}}_{n,i}(\mathbf{Y}_{n,i}), \cdot)\frac{\partial \dot{\mathbf{Y}}_{n,i}}{\partial \mathbf{Y}_{n,i}} + \frac{\partial \check{\mathbf{f}}}{\partial \mathbf{Y}_{n,i}}(\mathbf{Y}_{n,i}, \dot{\mathbf{Y}}_{n,i}(\mathbf{Y}_{n,i}), \cdot) \\ &= \frac{1}{\Delta t}\frac{\partial \check{\mathbf{f}}}{\partial \dot{\mathbf{Y}}_{n,i}}(\mathbf{Y}_{n,i}, \dot{\mathbf{Y}}_{n,i}(\mathbf{Y}_{n,i}), \cdot) + \frac{\partial \check{\mathbf{f}}}{\partial \mathbf{Y}_{n,i}}(\mathbf{Y}_{n,i}, \dot{\mathbf{Y}}_{n,i}(\mathbf{Y}_{n,i}), \cdot). \end{aligned} \tag{97}$$

Therefore, to solve the problem, two functions have to be defined in the PETSc module:

- $\check{\mathbf{f}}(\mathbf{y}, \dot{\mathbf{y}}, t)$,
- $\frac{\mathrm{d}\check{\mathbf{f}}}{\mathrm{d}\mathbf{y}}(\mathbf{y}, \dot{\mathbf{y}}, t)$.

The module includes strategies for adaptive timestepping based on local error estimates that will also be exploited.

7. Numerical results

The validation of the proposed numerical techniques constitutes a significant challenge due to the complexity of the coupled thermo-electrical-mechanical problem. For comparison purposes, neither experimental data are available, since they are difficult to obtain, nor benchmark examples capturing all the features of the proposed method have been found in the literature. Therefore, in order to assess the performance of the numerical techniques, four test problems with gradually increasing complexity have been solved. First, we address two manufactured test cases to determine the convergence rates of the numerical method. Subsequently, we simulate both a thermo-electrical-mechanical case and an in-die electric upsetting process to validate the numerical procedures for the fully coupled problem, comparing the results with those obtained using commercial software. The numerical implementation of the pure-Lagrangian method for the different examples is developed in a proprietary Python code based on the open-source finite element library FEniCS [30]. Let us recall that, since the Anand model considered in this work comprises a set of ordinary differential equations without any inequalities, this constitutive law and the equation for the displacement can be solved in a coupled manner, sharing the same discretization scheme. The variational form of this fully coupled model is defined in FEniCS's UFL language, which enables automatic discretization using the finite element method and the symbolic calculation of the system's Jacobian matrix.

Note that, while the inertia term is included in the general formulation of the motion equation for the sake of completeness, it is neglected throughout this section since this constitutes a plausible assumption in the present context.

The reference domain for the first three examples is a rectangle of radius R and length L, depicted in Fig. 7. The boundaries of this axisymmetric domain, $\hat{\Omega}$, are denoted as $\hat{\Gamma}_1$ ($z_m = 0$), $\hat{\Gamma}_2$ ($r_m = R$), $\hat{\Gamma}_3$ ($z_m = L$) and $\hat{\Gamma}_4$ ($r_m = 0$), such that $\partial\hat{\Omega} = \bigcup_{i=1}^{4} \hat{\Gamma}_i$. Notice that $\hat{\Gamma}_4$ coincides with the axis of symmetry. The values of R and L, as well as the boundary conditions, are specified for each example.

The material considered in this study is a typical steel, and the corresponding parameters used in the Anand model are listed in Table 1, where the deformation resistance at initial time has been prescribed.

In Examples 1 and 2, we compute the error between the discrete solution and a reference solution for temperature Θ, electric potential V, displacement $\mathbf{u}$, deformation resistance s, and plastic deformation gradient $\mathbf{F}^{\mathrm{p}}$. To achieve this, we approximate the theoretical H^1 and L^2 norms using a quadrature formula exact for polynomials of degree 1.

Table 1
Parameters used in the Anand model.

Parameter	A [s^{-1}]	Q [$Jmol^{-1}$]	ξ	h_0 [Pa]	$\bar{s}$ [Pa]	m	a	n	s^0 [Pa]
Value	10^{11}	$2.703 \cdot 10^5$	1.15	$13.29 \cdot 10^8$	$1.476 \cdot 10^8$	0.147	1	0.06869	$0.43 \cdot 10^8$

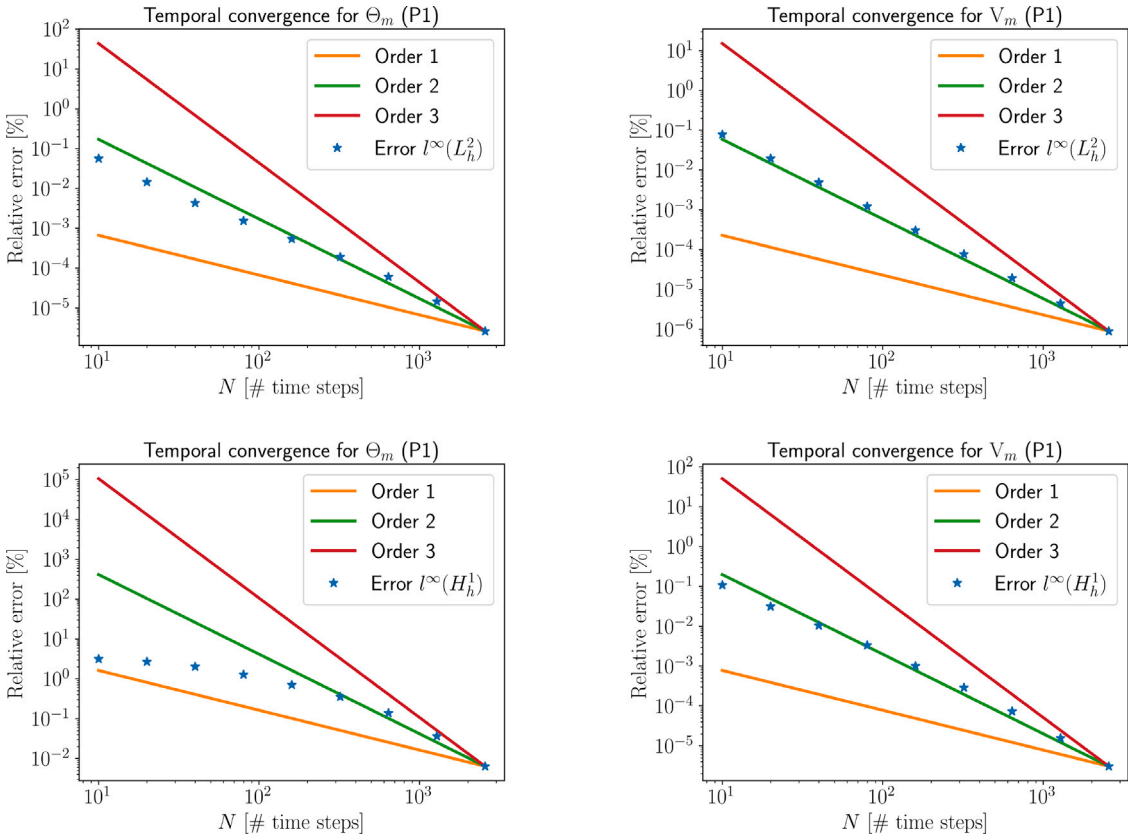

Fig. 8. Thermo-electrical manufactured problem: computed $l^\infty(L_h^2)$ (top) and $l^\infty(H_h^1)$ (bottom) errors for temperature (left) and voltage (right), versus the number of time steps, in log–log scale, for a fixed spatial mesh of size $h = 0.00125$.

Example 1 (*Thermo-electrical manufactured problem*)**.** This is an example aiming to check the rates of convergence of the scheme proposed in this paper applied to the thermo-electrical problem, where the deformation is assumed to be known, trying to emulate a typical electric upsetting. This displacement field and the computational domain are those from a previous article by the authors [17]. We note that the test considered in [17] was conducted to compare the implementations of both Eulerian and Lagrangian formulations of a thermo-electromagnetic problem, where an eddy current model [31] was used for the electromagnetic part. A completely different direct current model is now considered, and we focus on analyzing the spatial and time orders of convergence.

The electric direct current model and the thermal transient heat equation are considered in a cylinder of length $L = 0.165\,\mathrm{m}$ and radius $R = 0.02875\,\mathrm{m}$, with appropriate boundary conditions. Both models are coupled through the Joule effect and the temperature-dependent electrical properties, with initial and final times $t_0 = 0\,\mathrm{s}$ and $t_f = 20\,\mathrm{s}$. Let us consider a displacement vector field with a zero axial component and a radial component, $\widehat{u}_r(r_m, z_m)$, given by

$$\widehat{u}_r(r_m, z_m) = \begin{cases} 10^3 r_m \left(-188.2593 z_m + 6.1464\right) z_m^2 & \text{if } z_m \le 0.02, \\ r_m \left[1.0793 \exp\left(-\left(\dfrac{z_m - 0.0293}{0.03104}\right)^2\right) - 18.4974 \exp\left(-\left(\dfrac{z_m + 0.03324}{0.01705}\right)^2\right) + \right. & \\ \left. +1.0779 \exp\left(-\left(\dfrac{z_m - 0.4363}{1.263}\right)^2\right) - 1\right] & \text{if } z_m > 0.02. \end{cases}$$

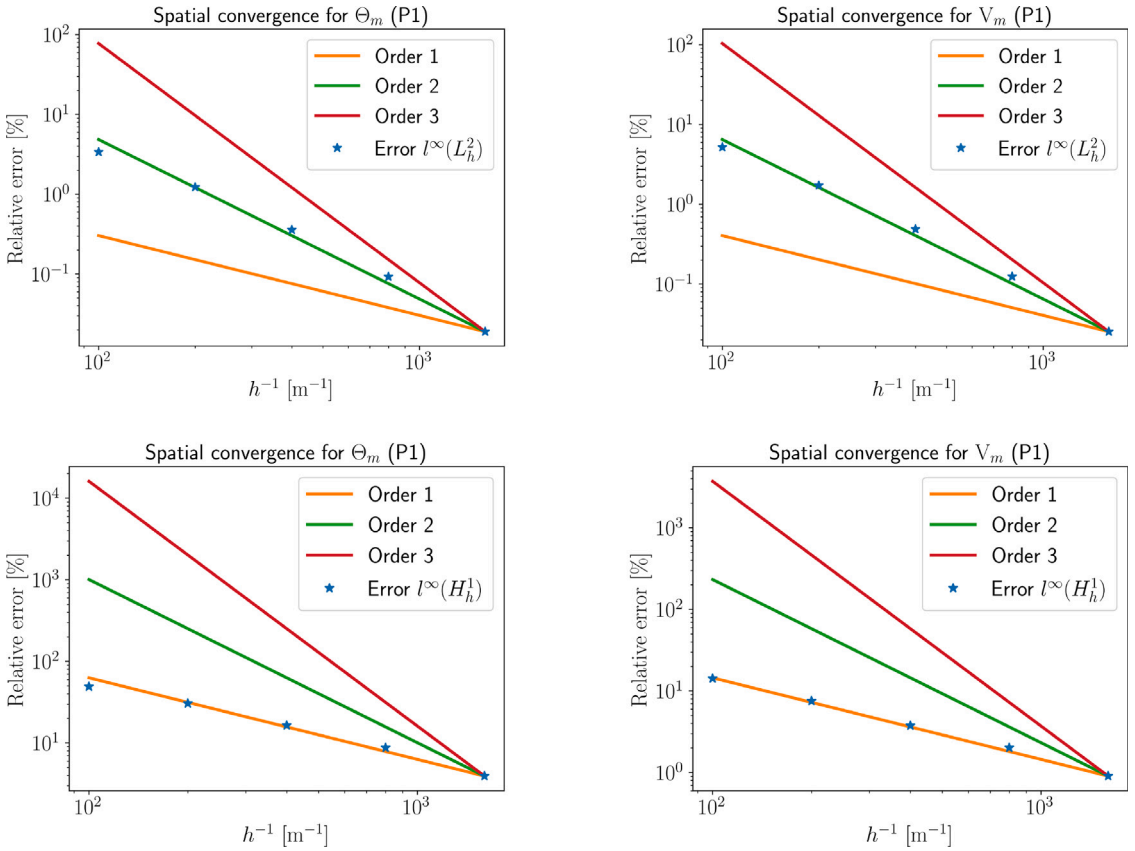

Fig. 9. Thermo-electrical manufactured problem: computed $l^\infty(L_h^2)$ (top) and $l^\infty(H_h^1)$ (bottom) errors for temperature (left) and voltage (right), versus $1/h$, in log–log scale, for $N = 20$.

The physical properties considered in this test are temperature-dependent functions which have been obtained in [17] by fitting tables of data corresponding to a typical steel. More precisely,

$$\check{\sigma}(\Theta) = \frac{1}{-4.3306\times10^{-13}\,(\Theta-273.15)^2 + 1.0839\times10^{-9}\,(\Theta-273.15) + 2.0170\times10^{-7}},$$

$$\check{k}(\Theta) = -2.7834\times10^{-11}\,(\Theta-273.15)^4 + 1.1045\times10^{-7}\,(\Theta-273.15)^3 - 1.3658\times10^{-4}\,(\Theta-273.15)^2 + 0.04639\,(\Theta-273.15) + 34.014,$$

$$\check{c}_p(\Theta) = 660.9\exp\left(-\left(\frac{\Theta-996.45}{23.93}\right)^2\right) + 288.9\exp\left(-\left(\frac{\Theta-970.75}{133.5}\right)^2\right) + 657.1\exp\left(-\left(\frac{\Theta-1181.25}{1497.0}\right)^2\right).$$

A constant mass density $\rho_m = 7799\ \mathrm{kg\,m^{-3}}$ is considered. Concerning the thermal model, we impose null heat flux on the symmetry boundary $\hat{\Gamma}_4$, and convection and radiation conditions on $\hat{\Gamma}_1$, $\hat{\Gamma}_2$ and $\hat{\Gamma}_3$, with a heat transfer coefficient $h = 20\ \mathrm{W\,m^{-2}\,K^{-1}}$, convection temperature $\hat{\Theta}^C = 295.15$ K, emissivity $\epsilon = 0.9$, radiation temperature $\hat{\Theta}^R = 303.15$ K. The initial temperature $\hat{\Theta}^0 = 300$ K is considered.

For the direct current model, we impose a null electric potential on $\hat{\Gamma}_1$, and a given normal electrical current density is prescribed on $\hat{\Gamma}_3$, namely, $\mathbf{J}\cdot\mathbf{n} = -4\times10^{10} r_m^2$. Notice that r_m is the radial coordinate and the current travels from $\hat{\Gamma}_3$ to $\hat{\Gamma}_1$. On $\hat{\Gamma}_2$ and $\hat{\Gamma}_4$, tangential electrical current is considered (natural Neumann boundary condition).

This problem has been solved by using a second-order method of the ARKIMEX family, namely, the ARKIMEX L2 method. Moreover, for space discretization, we have considered continuous piecewise-linear finite elements for both temperature and electric potential.

In Fig. 8 we fix the spatial mesh and show $l^\infty(L_h^2)$ and $l^\infty(H_h^1)$ errors for temperature and voltage as a function of the number of time steps. A reference solution computed with a finer time step ($N = 5120$) and mesh-size ($h = 0.00125$) is used for comparison. We can observe that the scheme shows second-order accuracy in time for temperature and voltage.

In Fig. 9 we represent the computed $l^\infty\left(L_h^2\right)$ and $l^\infty\left(H_h^1\right)$ errors for temperature and voltage as functions of $1/h$, using a fixed small time step, namely $N = 20$. A reference solution obtained with $N = 20$ and $h = 0.0003125$ has been used for comparison. We can observe that the scheme possesses second-order accuracy in space in the $l^\infty(L_h^2)$-norm and first-order accuracy in space in the $l^\infty(H_h^1)$-norm. Error estimations for a stationary thermo-electrical model can be found in [32], and the reported spatial convergence order is consistent with the results presented.

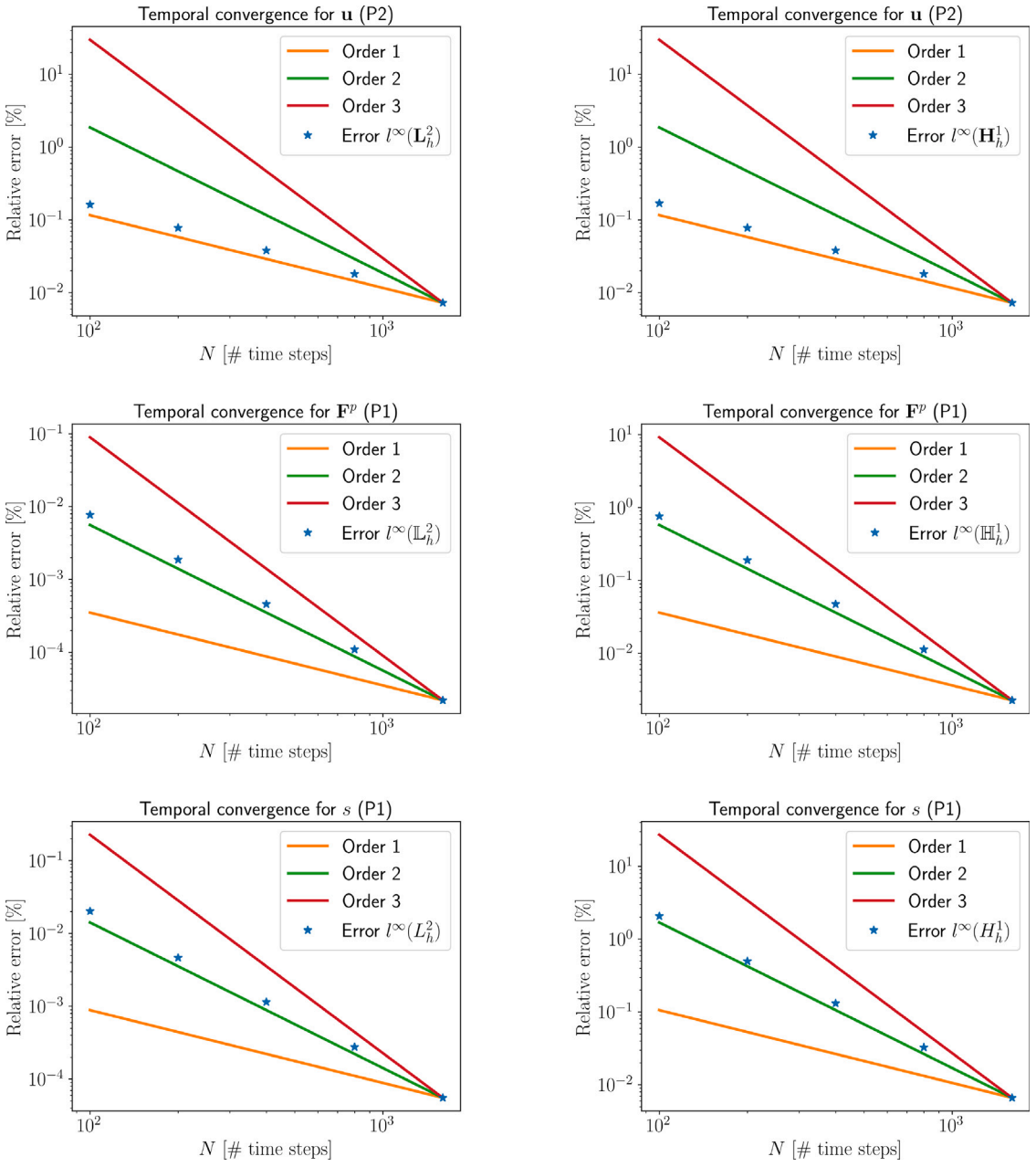

Fig. 10. Mechanical manufactured problem: computed $l^\infty(L^2_h)$ (left) and $l^\infty(H^1_h)$ (right) errors for displacement, plastic deformation gradient and deformation resistance, versus the number of time steps, in log–log scale, for a fixed spatial mesh of size $h = 0.0025$.

Example 2 (*Mechanical manufactured problem*)**.** This is an example aiming to check the rates of convergence of the proposed scheme applied to an elasto-viscoplastic mechanical problem in the axisymmetric rectangular domain $\widehat{\Omega} = (0, 0.025) \times (0.25, 0.375)$, such that $L = 0.125$ m and $R = 0.025$ m. The time interval is $[t_0, t_f] = [0\,\text{s}, 100\,\text{s}]$. A non-uniform temperature distribution is considered:

$$\Theta_m(\mathrm{p}, t) = -17600 z_m^2 + 8800 z_m + 300.$$

The elastic parameters $\check{E}$ (Young's modulus) and $\check{\nu}$ (Poisson's ratio) are temperature-dependent. More precisely,

$$\check{E}(\Theta) = 1.333 \times 10^{11} \sin\left(1.005 \times 10^{-6}\Theta + 0.958\right) + 1.072 \times 10^{11} \sin\left(2.159 \times 10^{-3}\Theta + 0.879\right) + \\ + 1.323 \times 10^{10} \sin\left(7.401 \times 10^{-3}\Theta + 1.254\right),$$

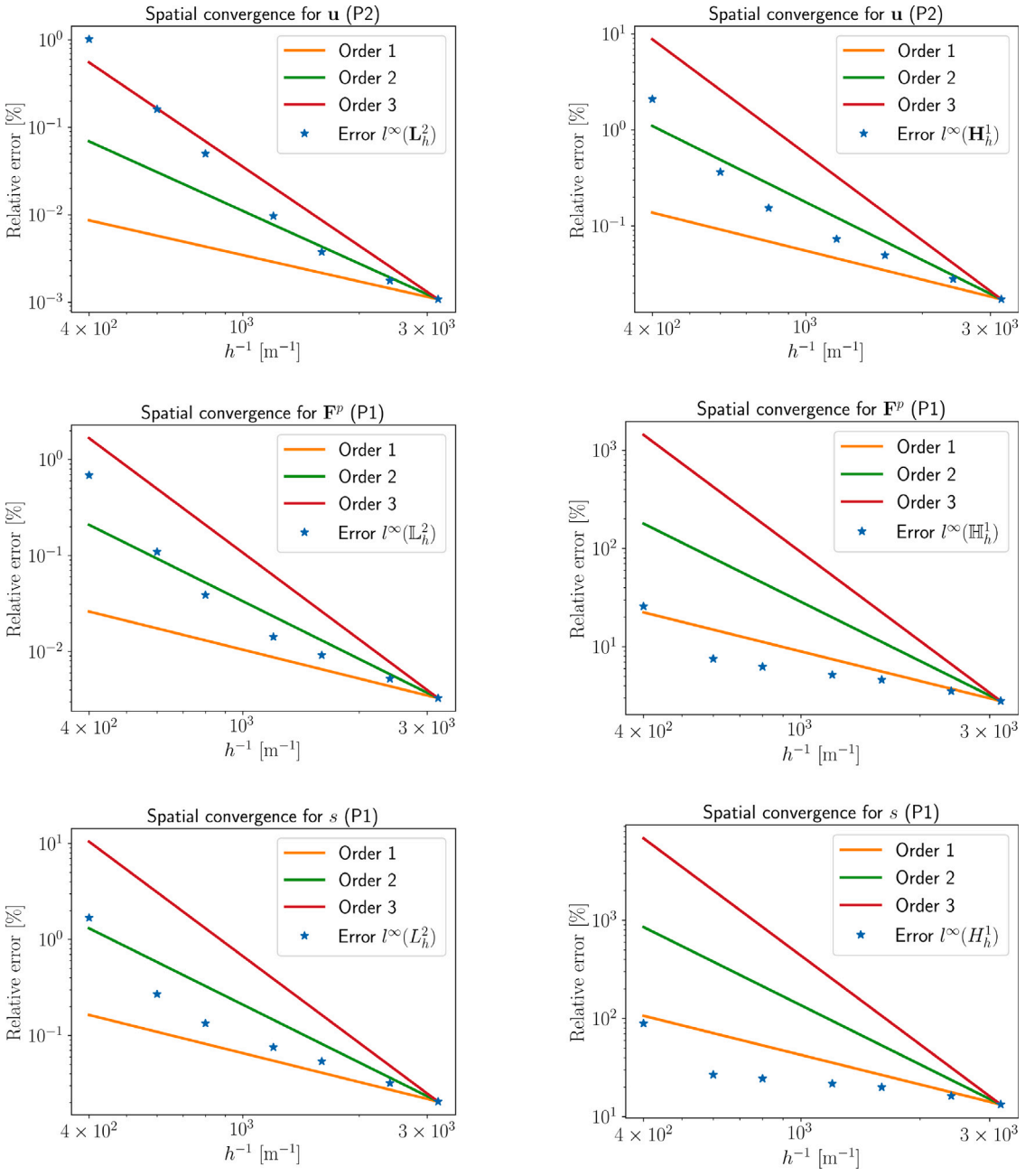

Fig. 11. Mechanical manufactured problem: computed $l^\infty(L^2_h)$ (left) and $l^\infty(H^1_h)$ (right) errors for displacement, plastic deformation gradient and deformation resistance, versus $1/h$, in log–log scale, for $N = 100$.

$$\check{\nu}(\Theta) = \begin{cases} 6.353 \times 10^{-10}\Theta^{2.602} + 0.2828 & \text{if } \Theta \leq 923.15, \\ 0.3158 & \text{if } \Theta > 923.15. \end{cases}$$

To satisfy symmetry conditions, zero normal displacements are enforced on boundaries $\hat{\Gamma}_1$ and $\hat{\Gamma}_4$. On $\hat{\Gamma}_2$ a null Neumann condition (force-free) is imposed while a non-follower force is applied over time on $\hat{\Gamma}_3$, namely,

$$\mathbf{P}(t) = \pi(0.025)^2 \times 5.5 \times 10^7 \frac{\ln(1 - 0.005t)}{1 - 0.005t}\mathbf{e}_z.$$

This problem has been solved using the second order ARKIMEX L2 method. Moreover, for space discretization, we have considered continuous piecewise-linear finite elements for each plastic deformation gradient component F^{p}_{ij} and for the deformation resistance s, while continuous piecewise quadratic elements are used for each displacement component.

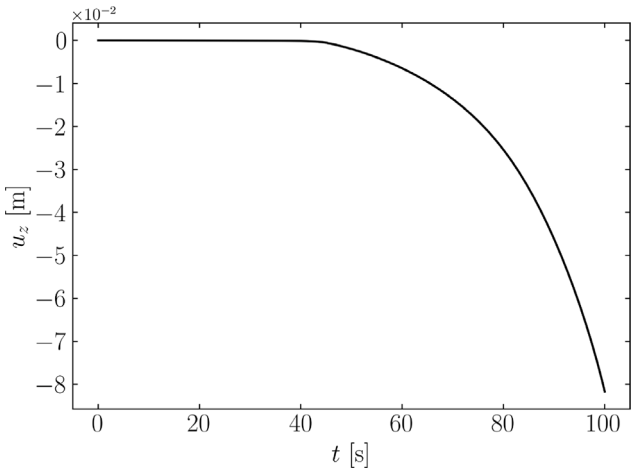

Fig. 12. Thermo-electrical-mechanical problem: normal displacement prescribed on $\hat{\Gamma}_3$.

In Fig. 10 we fix the spatial mesh and show the $l^\infty(L_h^2)$ and $l^\infty(H_h^1)$ errors for displacement, plastic deformation gradient and deformation resistance, as function of the number of time steps. A reference solution computed with a finer time step ($N = 3200$) and mesh-size ($h = 0.0025$) is used for comparison. The results demonstrate that the scheme achieves second-order accuracy in time for plastic deformation gradient and deformation resistance and first-order accuracy in time for displacement.

In Fig. 11 we represent the computed $l^\infty\left(L_h^2\right)$ and $l^\infty\left(H_h^1\right)$ errors for displacement, plastic deformation gradient and deformation resistance, as functions of $1/h$, using a fixed small time step, namely, $N = 100$. A reference solution obtained with $N = 100$ and $h = 0.00015625$ has been used for comparison. The results indicate that the scheme achieves second-order accuracy in space for the $l^\infty(L_h^2)$-norm and first-order accuracy in space for the $l^\infty(H_h^1)$-norm.

Example 3 (*Thermo-electrical-mechanical problem*)**.** In this example, a fully coupled thermo-electrical-mechanical model is solved in the axisymmetric rectangular domain $\hat{\Omega} = (0, 0.025) \times (0, 0.25)$. The time interval is $[t_0, t_f] = [0\,\text{s}, 100\,\text{s}]$. The thermal, electrical and elasto-viscoplastic mechanical properties are those used in Examples 1 and 2.

A symmetry condition (zero normal displacement) is enforced on $\hat{\Gamma}_4$ and a force-free condition is assumed on $\hat{\Gamma}_2$. Mechanical contact is considered on $\hat{\Gamma}_1$. Moreover, the normal component of the displacement shown in Fig. 12 is imposed over time on $\hat{\Gamma}_3$.

Regarding the thermal model, null heat flux is imposed on the symmetry boundary $\hat{\Gamma}_4$, and convection is considered on $\hat{\Gamma}_2$ and $\hat{\Gamma}_3$, with a heat transfer coefficient $h = 20\ \text{W m}^{-2}\,\text{K}^{-1}$ and convection temperature $\hat{\Theta}^C = 300$ K. Moreover, a Dirichlet boundary condition is considered on $\hat{\Gamma}_1$ with fixed temperature $\hat{\Theta}^{DT} = 500$ K. The initial temperature $\hat{\Theta}^0 = 273.15$ K is considered in the whole domain.

For the direct current model, null electric potential is imposed on $\hat{\Gamma}_1$. In addition, a constant electric potential $\hat{V}^{DE} = 0.8$ V is fixed on a part of $\hat{\Gamma}_2$, between $z_m = 0.175$ m and $z_m = 0.2$ m. Elsewhere on the boundaries, tangential electrical current is considered (natural Neumann boundary condition).

Concerning the time discretization, this problem has been solved using the third order ARKIMEX 3 method. In addition, for space discretization, we have considered continuous piecewise-linear finite elements for each plastic deformation gradient component F_{ij}^{p}, for the deformation resistance s, the temperature and the electric potential, while continuous piecewise quadratic elements are used for each displacement component.

The proposed pure-Lagrangian (PL) method was applied to this problem and compared with solutions obtained using the commercial software Ansys and Marc. In Figs. 13, 14 and 15 we present the temperature distributions on the deformed domain at several time instants, computed with our method as well as those obtained using Ansys and Marc. Additionally, in Fig. 16 we show the evolution of several magnitudes at the midpoint of the symmetry boundary, $(r_m, z_m) = (0\,\text{m}, 0.125\,\text{m})$, along with the evolution of the maximum radial displacement. The results demonstrate good agreement among the different solvers. In fact, in order to quantify the accuracy of the comparison, the following error is computed between the results obtained using the proposed pure-Lagrangian method, and those from the two commercial solvers:

$$100\ \frac{1}{N}\sum_{i=1}^{N}\left|\frac{A_i^{\text{Ansys/Marc}} - A_i^{\text{PL}}}{A_i^{\text{Ansys/Marc}}}\right|, \tag{98}$$

where A refers to the specific magnitude in Fig. 16 for which the error is computed, the subscript i refers to the simulation time t_i, the superscript denotes the solver and N is the total number of time instants. Note that linear interpolation is previously used to have the same time instants for all the solvers. Moreover, contributions resulting from division by values $A_i^{\text{Ansys/Marc}}$ smaller than 10^{-4} are omitted in order not to distort the error for ϵ^p and u_r^{max} in the initial part of the corresponding curves. The resulting errors are summarized in Table 2.

Table 2
Comparative errors computed according to Eq. (98) for the modulus of the current density, the temperature and the accumulated inelastic strain at $(r_m, z_m) = (0\,\text{m}, 0.125\,\text{m})$, and for the maximum radial displacement.

Comparison	Error $\|\mathbf{J}\|$ (%)	Error Θ (%)	Error e^p (%)	Error u_r^{max} (%)
PL vs Ansys	1.24	1.48	8.27	2.85
PL vs Marc	0.07	0.02	2.00	3.81

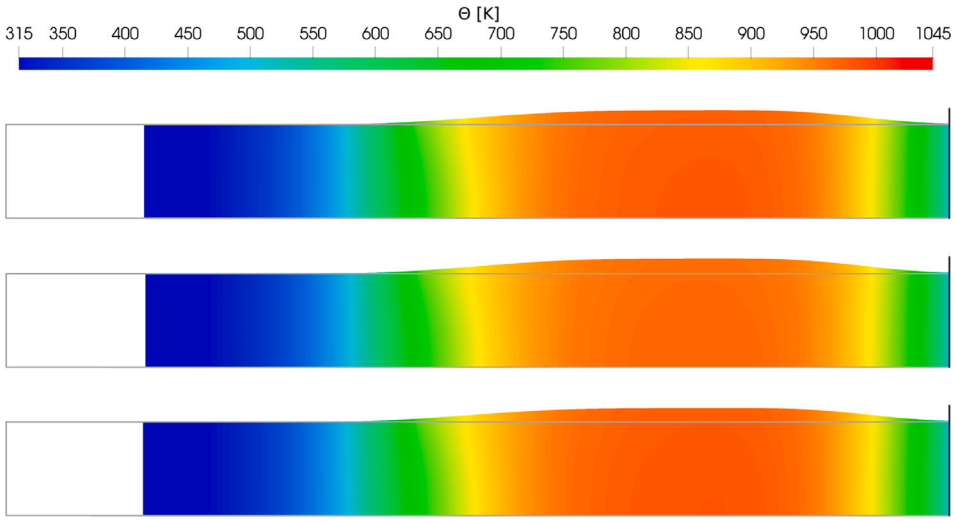

Fig. 13. Thermo-electrical-mechanical problem: temperature and deformed domain (the reference domain is outlined in grey) at $t = 85\,\text{s}$, computed using the proposed pure-Lagrangian method (top), Ansys (middle) and Marc (bottom).

In order to accurately simulate large strain problems involving viscoplastic deformations, the finite element mesh to be used must have enough quality and refinement level, since the element distortion can become severe in the most deformed regions. This fact is appreciated in Fig. 17, where the Frobenius norm of the plastic deformation gradient at the final time is shown, with a detailed view of the mesh in the deformed domain.

Example 4 (*In-die electric upsetting*)**.** Electric upsetting is a multiphysics metal forming process characterized by large deformations and rapid changes in temperature caused by electrical heating in the workpiece, typically a steel bar. This process is widely employed in the manufacturing of automotive pieces, particularly axle shafts, which are integral to the transmission system of different types of vehicles, including cars, vans or buses. The ends of axle shafts are produced using electric upsetting processes, either in free form or within a closed die, depending on the specific requirements.

The pinion section of the axle shaft is formed through an in-die electric upsetting process, which aims to thicken one end of the steel bar. This process begins with a low-voltage, high-amperage electrical current passing through the bar end, between the electrical contacts of the anvil and the gripper, lasting for 11 s. Over the next 23 s, the anvil retracts to create space for the bar end to expand. Finally, during the last 29 s, the upsetting cylinder pushes the opposite end of the bar, causing it to widen and fill the die. Fig. 18 provides a simplified diagram of the main components involved in this process.

This example has been selected to demonstrate the capabilities of the proposed numerical scheme for modeling an in-die electric upsetting process applied to a steel bar. Initially, the bar has a diameter of 44 mm and a length of 1290 mm, while the die has a diameter of 52.4 mm. The initial geometry and boundary conditions for the coupled problem are depicted in Fig. 19, where a dashed line identifies the symmetry boundary, denoted as $\hat{\Gamma}^6$. A force is applied on $\hat{\Gamma}^5$, namely,

$$\mathbf{P}(t) = \pi(0.022)^2 \times \begin{cases} -\dfrac{5833035}{34} t\mathbf{e}_z & \text{if } t < 34, \\ 172657836 - \dfrac{10499463}{2} t\mathbf{e}_z & \text{if } 34 \le t \le \dfrac{346}{9}, \\ -\dfrac{58330350}{1+\exp\left(\frac{346}{25} - \frac{9}{25}t\right)}\mathbf{e}_z & \text{if } t > \dfrac{346}{9}. \end{cases}$$

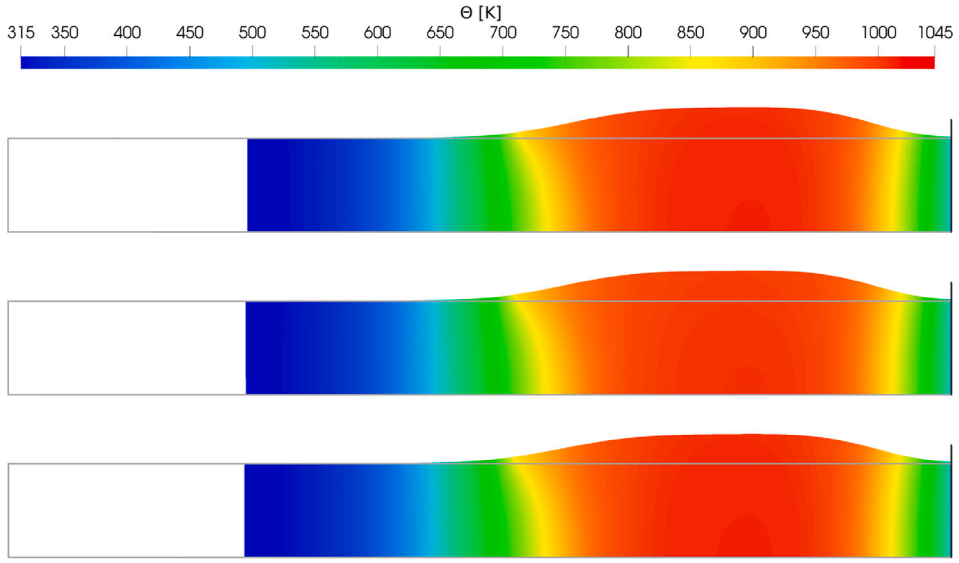

Fig. 14. Thermo-electrical-mechanical problem: temperature and deformed domain (the reference domain is outlined in grey) at $t = 95\,\mathrm{s}$, computed using the proposed pure-Lagrangian method (top), Ansys (middle) and Marc (bottom).

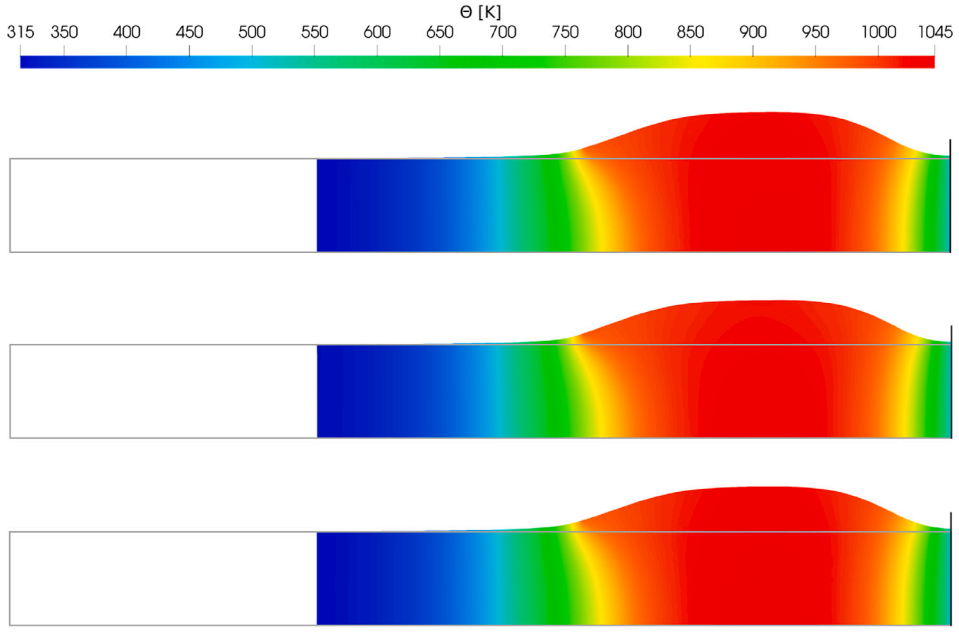

Fig. 15. Thermo-electrical-mechanical problem: temperature and deformed domain (the reference domain is outlined in grey) at $t = 100\,\mathrm{s}$, computed using the proposed pure-Lagrangian method (top), Ansys (middle) and Marc (bottom).

In addition, a convective-radiative heat flux boundary condition is considered on $\bigcup_{i=2}^{5} \widehat{\Gamma}^i$ with $h = 20\,\mathrm{Wm^{-2}K^{-1}}$, $\Theta^C = 295.15\,\mathrm{K}$, $\Theta^R = 303.15\,\mathrm{K}$ and $\epsilon = 0.9$, while convective heat flux boundary condition with $h = 10^5\ \mathrm{Wm^{-2}K^{-1}}$, $\Theta^C = 495.15\,\mathrm{K}$ is imposed on $\widehat{\Gamma}^1$.

Regarding the electrical problem, the potential depicted in Fig. 20 is applied on $\widehat{\Gamma}^3$. The reference (null) electric potential is imposed on $\widehat{\Gamma}^1$, while a null Neumann condition is applied on the rest of the boundaries. Notably, due to the backward movement of the anvil, the electric potential depicted in Fig. 20 is imposed only on a time-dependent part of $\widehat{\Gamma}^3$ with a length matching that of the gripper. Additionally, an obstacle associated with the anvil is considered, which necessitates adjustments to the boundary conditions when the contact takes place. Specifically, we impose a null electric potential and a convective heat flux boundary condition with $h = 10^4\,\mathrm{Wm^{-2}K^{-1}}$, $\Theta^C = 473.15\,\mathrm{K}$, on the part of the boundary that is in contact with the obstacle. Fig. 21 illustrates the current density across four instantaneous configurations of the (Eulerian) domain.

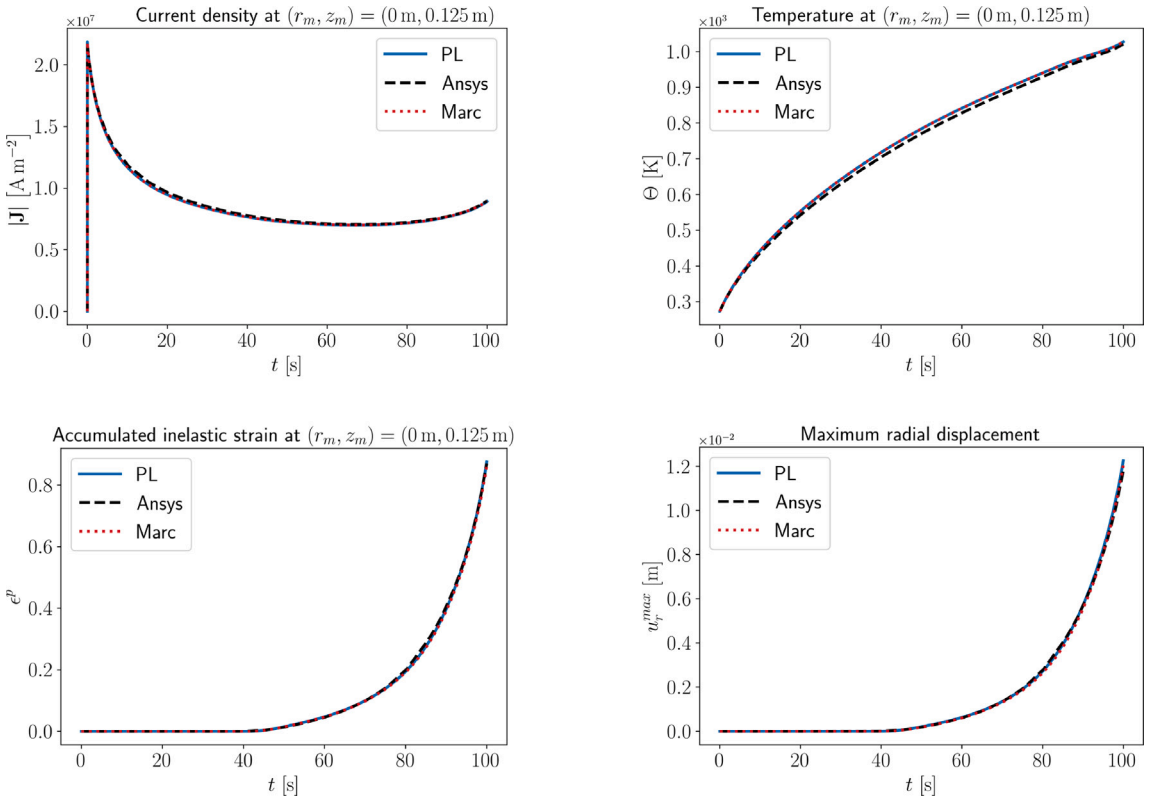

Fig. 16. Thermo-electrical-mechanical problem: time evolution of the modulus of the current density (top left), the temperature (top right) and the accumulated inelastic strain (bottom left) at $(r_m, z_m) = (0\,\mathrm{m}, 0.125\,\mathrm{m})$ and maximum radial displacement (bottom right).

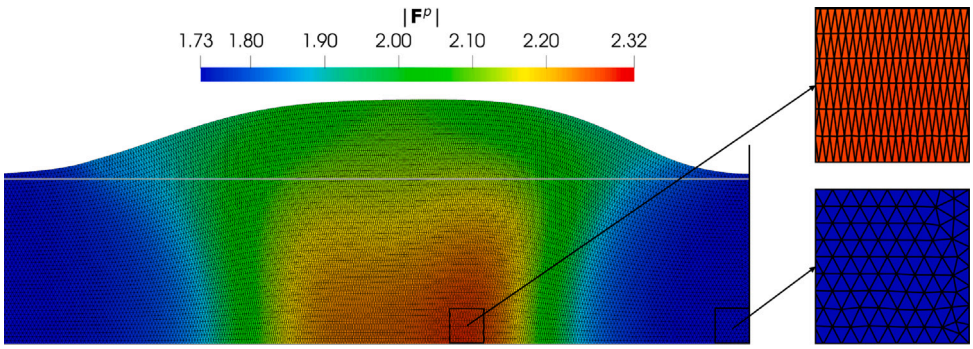

Fig. 17. Thermo-electrical-mechanical problem: Frobenius norm of the plastic deformation gradient and deformed mesh (the reference domain is outlined in grey) at $t = 100\,\mathrm{s}$, computed using the proposed pure-Lagrangian method. Note the mesh distortion over the most deformed area (zoom in the right image), since the initial mesh is almost uniform with similar size to that of the blue zone.

This problem was also solved using the commercial software packages Ansys and Marc, with results that closely match those obtained with our numerical code. The results from Marc, Ansys, and our method are depicted in Figs. 22–25, showing the temperature distribution and the geometry at four different times. It is worth noting that achieving an accurate solution with the Marc code required a smaller time step compared to our method and the Ansys code. In Ansys, an updated Lagrangian method is used to solve the mechanical problem, where the discrete equations are formulated based on the configuration from the previous time step. Additionally, Ansys employs a staggered approach in which a unified code independently solves the electrical, mechanical, and thermal problems. Conversely, the Marc code adopts an Eulerian framework, which involves recalculating the computational domain and reinitializing the motion at each time step. Both strategies demand computational overhead to update and maintain the domain at each time step.

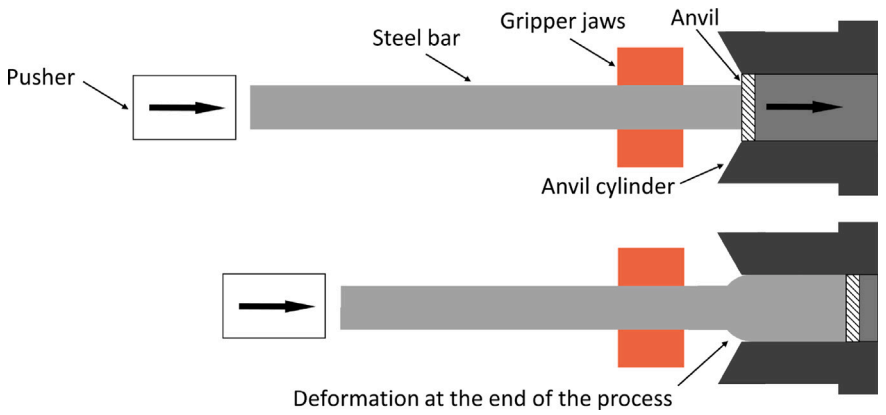

Fig. 18. In-die electric upsetting: sketch of the elements considered in the process.

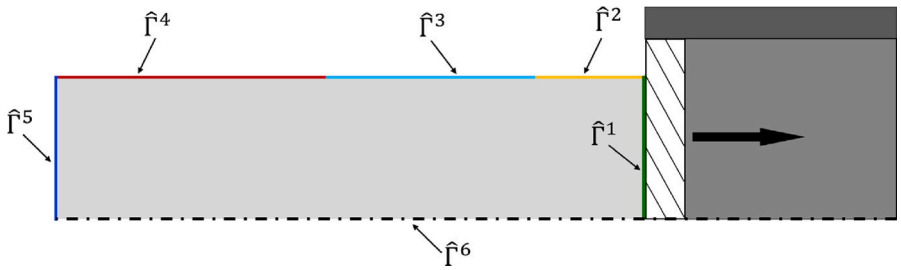

Fig. 19. In-die electric upsetting: initial geometry and boundary conditions.

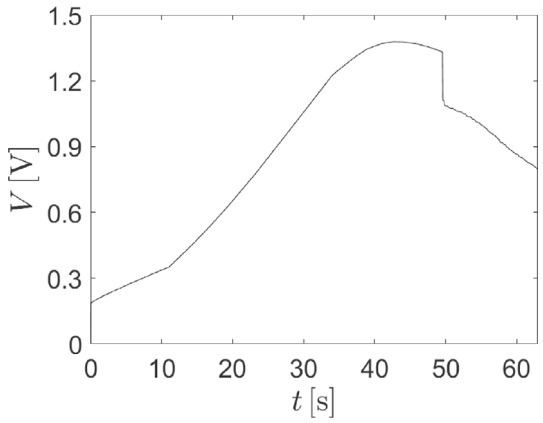

Fig. 20. In-die electric upsetting: electric potential prescribed on $\hat{\Gamma}^3$.

8. Conclusions

In this work, we have described a numerical approach for solving a fully coupled thermo-electrical-mechanical model, which was motivated by the modeling and simulation of electrically assisted forming processes. Our methodology is based on pure-Lagrangian formulations, which allows us to work with a time-independent and predefined computational domain and to avoid updating the mesh at each time step. We proposed a fully discrete scheme combining finite elements for spatial discretization and Runge–Kutta methods for time integration. From a modeling standpoint, we selected an elasto-viscoplastic model for large deformations and incorporated appropriate contact boundary conditions. We developed our own Python-FEniCS code implementation and performed several numerical tests in axisymmetric geometries to ensure its proper validation. In particular, different academic tests of increasing difficulty were performed, as well as comparisons with solutions obtained from our code and from commercial software for a thermo-electrical-mechanical case, and a specific in-die electric upsetting process. The computed results closely align with those obtained from commercial simulation tools, demonstrating the effectiveness of the approach.

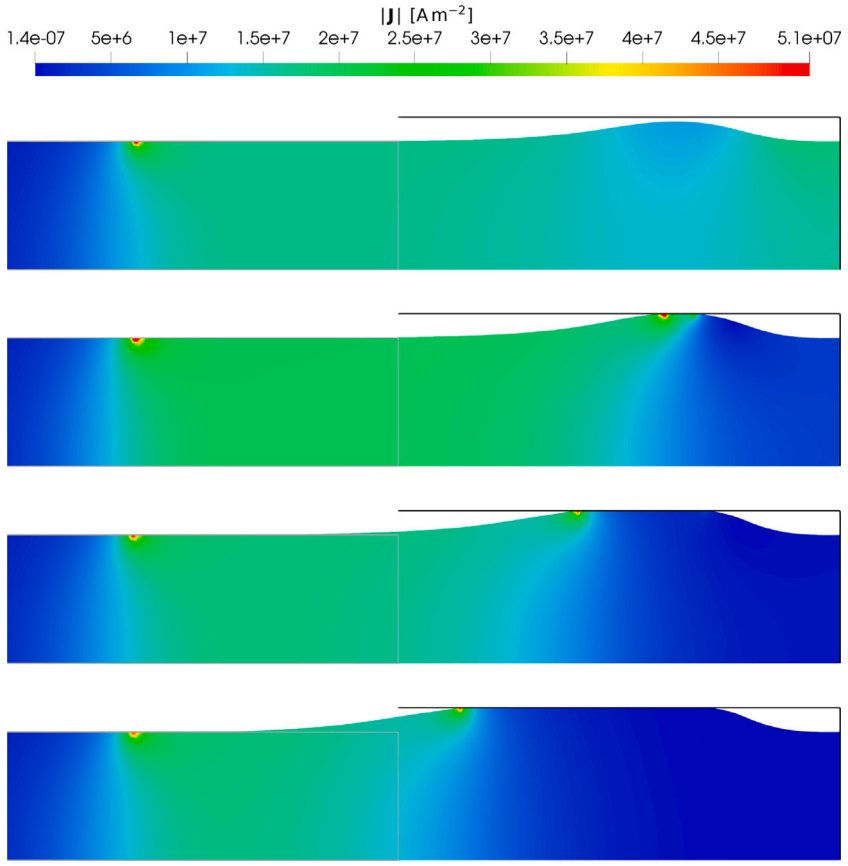

Fig. 21. In-die electric upsetting: modulus of the current density and deformed domain (the reference domain is outlined in grey) at $t = 46$ s, $t = 48$ s, $t = 54$ s, $t = 63$ s, computed using the proposed pure-Lagrangian method.

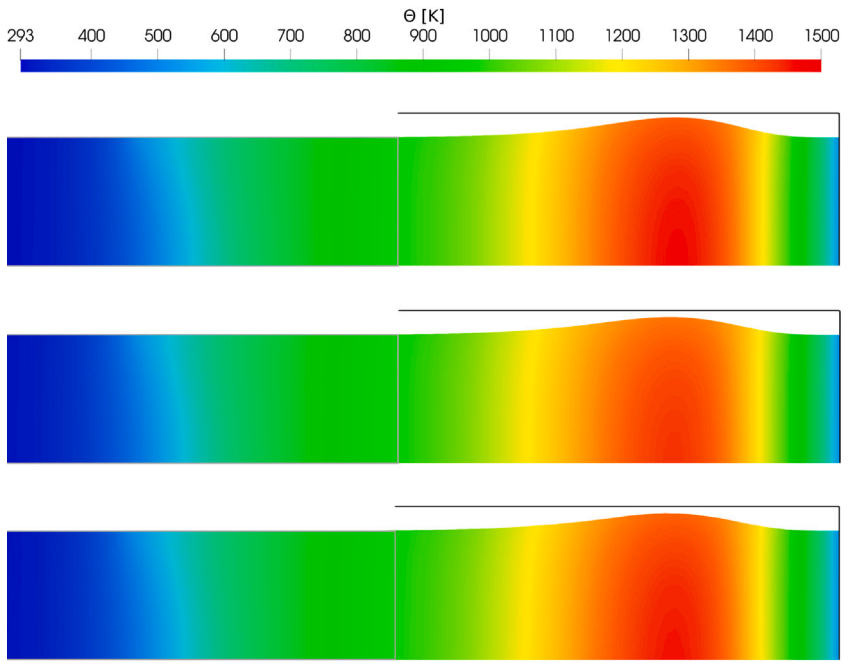

Fig. 22. In-die electric upsetting: temperature and deformed domain (the reference domain is outlined in grey) at $t = 46$ s, computed using the proposed pure-Lagrangian method (top), Ansys (middle) and Marc (bottom).

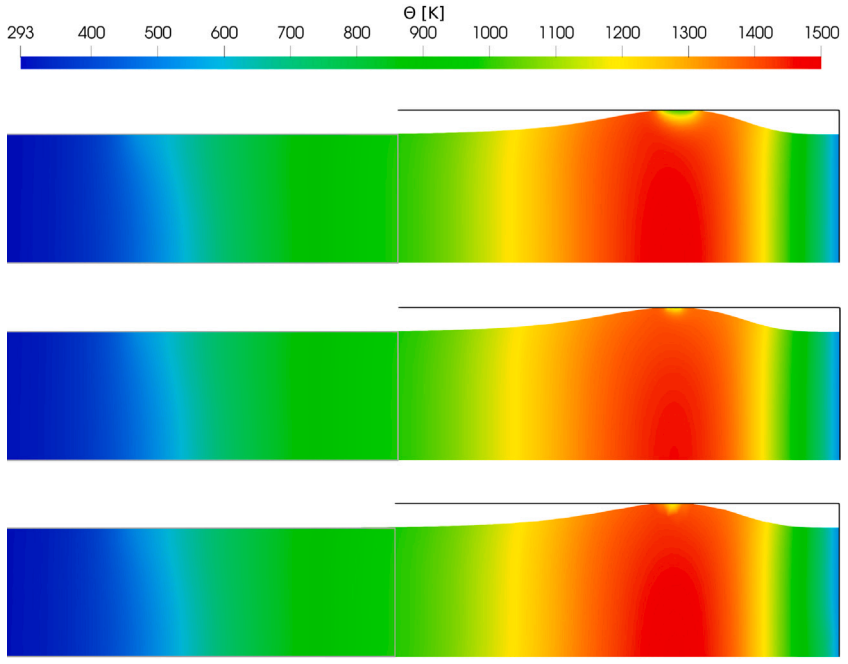

Fig. 23. In-die electric upsetting: temperature and deformed domain (the reference domain is outlined in grey) at $t = 48\,\mathrm{s}$, computed using the proposed pure-Lagrangian method (top), Ansys (middle) and Marc (bottom).

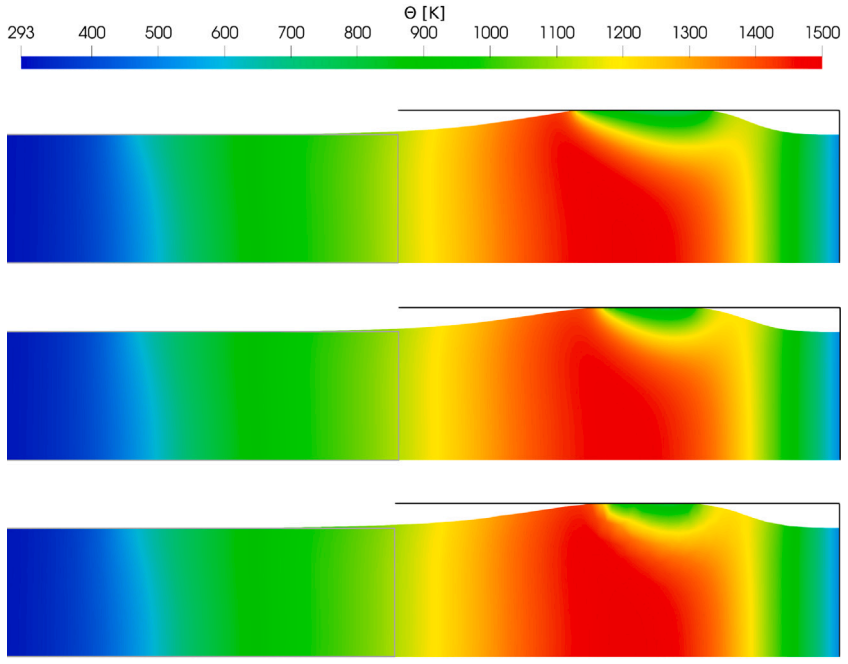

Fig. 24. In-die electric upsetting: temperature and deformed domain (the reference domain is outlined in grey) at $t = 54\,\mathrm{s}$, computed using the proposed pure-Lagrangian method (top), Ansys (middle) and Marc (bottom).

We have focused on a specific elasto-viscoplastic model, but our methodology can be expanded by considering different constitutive laws, which we are exploring. Moreover, the proposed model could also be extended to address the simulation of different electrically assisted forming processes. Regarding the numerical side, we plan to develop robust reinitialization and remeshing techniques, which may be necessary when the mesh becomes highly distorted.

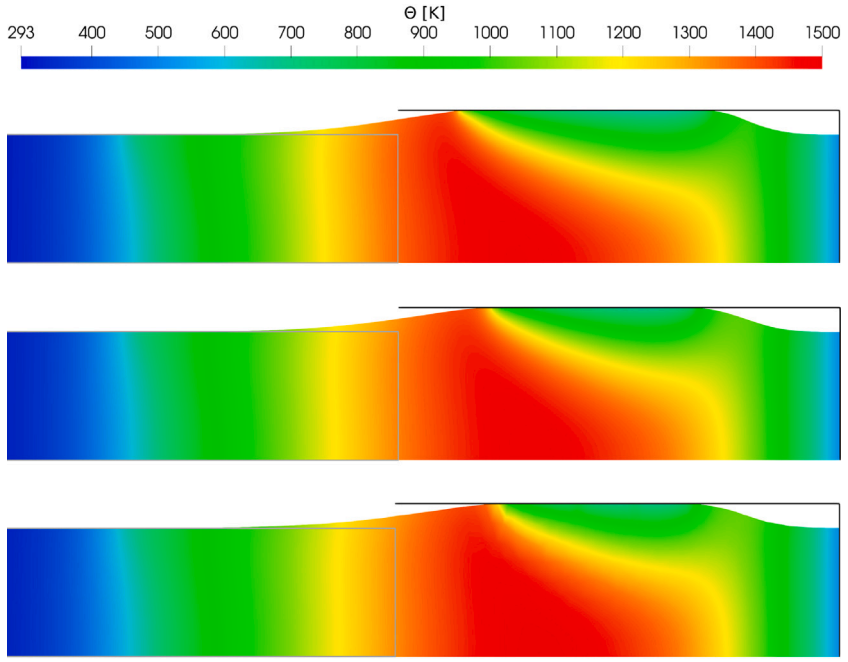

Fig. 25. In-die electric upsetting: temperature and deformed domain (the reference domain is outlined in grey) at $t = 63\,\mathrm{s}$, computed using the proposed pure-Lagrangian method (top), Ansys (middle) and Marc (bottom).

CRediT authorship contribution statement

M. Benítez: Writing – original draft, Methodology, Investigation. **A. Bermúdez:** Writing – review & editing, Methodology, Investigation. **P. Fontán:** Writing – review & editing, Software, Methodology. **I. Martínez:** Writing – review & editing, Software, Methodology. **P. Salgado:** Writing – review & editing, Methodology, Investigation, Funding acquisition.

Funding

The research has been developed in collaboration with CIE Galfor through a project granted by the Centre for the Development of Industrial Technology (CDTI) and signed between the company CIE Galfor and Itmati (nowadays, integrated in CITMAga). This work has been partially funded by MCIN /AEI /10.13039/501100011033/FEDER, UE under research Project PID2021-122625OB-I00.

Declaration of competing interest

The authors declare that they have no known competing financial interests or personal relationships that could have appeared to influence the work reported in this paper.

Data availability

The data used for the research is described in the article.

References

[1] J. Alves, S. Acevedo, S. Marie, B. Adams, K. Mocellin, F. Bay, Numerical modeling of electrical upsetting manufacturing processes based on Forge environment, AIP Conf. Proc. 1896 (2017).
[2] G.Z. Quan, Z.Y. Zou, Z.H. Zhang, J. Pan, A study on formation process of secondary upsetting defect in electric upsetting and optimization of processing parameters based on multi-field coupling FEM, Mater. Res. 19 (2016).
[3] R.E. Ewing, H. Wang, A summary of numerical methods for time-dependent advection-dominated partial differential equations, J. Comput. Appl. Math. 128 (2001) 423–445.
[4] M. Benítez, A. Bermúdez, A second order characteristics finite element scheme for natural convection problems, J. Comput. Appl. Math. 235 (2011) 3270–3284.
[5] K. Boukir, Y. Maday, B. Métivet, E. Razafindrakoto, A high-order characteristics/finite element method for the incompressible Navier-Stokes equations, Intern. J. Numer. Methods Fluids 25 (1997) 1421–1454.

[6] J. Douglas, Jr., T.F. Russell, Numerical methods for convection-dominated diffusion problems based on combining the method of characteristics with finite element or finite difference procedures, SIAM J. Numer. Anal. 19 (1982) 871–885.
[7] R.E. Ewing, T.F. Russel, Multistep Galerkin methods along characteristics for convection-diffusion problems, in: Advances in Computer Methods for Partial Differential Equations, vol. IV, IMACS Publications, 1981, pp. 28–36.
[8] O. Pironneau, On the transport-diffusion algorithm and its applications to the Navier-Stokes equations, Numer. Math. 38 (1982) 309–332.
[9] H. Rui, M. Tabata, A second order characteristic finite element scheme for convection-diffusion problems, Numer. Math. 92 (2002) 161–177.
[10] E. Süli, Stability and convergence of the Lagrange-Galerkin method with non-exact integration, in: The Mathematics of Finite Elements and Applications, vol. VI, Academic Press, London, 1988, pp. 435–442,
[11] M. Benítez, A. Bermúdez, Numerical analysis of a second-order pure Lagrange-Galerkin method for convection-diffusion problems. Part I: time discretization, SIAM. J. Numer. Anal. 50 (2012) 858–882.
[12] M. Benítez, A. Bermúdez, Numerical analysis of a second-order pure Lagrange-Galerkin method for convection-diffusion problems. Part II: fully discretized scheme and numerical results, SIAM. J. Numer. Anal. 50 (2012) 2824–2844.
[13] M. Benítez, A. Bermúdez, Pure Lagrangian and semi-Lagrangian finite element methods for the numerical solution of convection-diffusion problems, Int. J. Numer. Anal. Mod. 11 (2014) 271–287.
[14] M. Benítez, A. Bermúdez, Pure Lagrangian and semi-Lagrangian finite element methods for the numerical solution of Navier-Stokes equations, Appl. Numer. Math. 95 (2015) 62–81.
[15] M. Benítez, A. Bermúdez, Second order pure Lagrange-Galerkin methods for fluid-structure interaction problems, SIAM J. Sci. Comput. 37 (2015) B744–B777.
[16] M. Benítez, A. Bermúdez, P. Fontán, Non-Eulerian Newmark methods: A powerful tool for free-boundary continuum mechanics problems, J. Sci. Comput. 83 (2020) 1–27.
[17] M. Benítez, A. Bermúdez, P. Fontán, I. Martínez, P. Salgado, A Lagrangian approach for solving an axisymmetric thermo-electromagnetic problem. Application to time-varying geometry processes, Adv. Comput. Math. 50 (2024).
[18] I. Niyonzima, Y. Jiao, J. Fish, Modeling and simulation of nonlinear electro-thermo-mechanical continua with application to shape memory polymeric medical devices, Comput. Methods Appl. Mech. Engrg. 350 (2019) 511–534.
[19] G. Weber, L. Anand, Finite deformation constitutive equations and a time integration procedure for isotropic, hyperelastic-viscoplastic solids, Comput. Methods Appl. Mech. Engrg. 79 (1990).
[20] M.E. Gurtin, An Introduction to Continuum Mechanics, vol. 158, Academic Press, San Diego, Academic Press, San Diego, 1981.
[21] H. Yang, X.C. Cai, Parallel two-grid semismooth Newton-Krylov-Schwarz method for nonlinear complementarity problems, J. Sci. Comput. 47 (2011).
[22] J. Simo, Numerical analysis and simulation of plasticity, in: Numerical Methods for Solids (Part 3) Numerical Methods for Fluids (Part 1), in: Handbook of Numerical Analysis, vol. 6, Elsevier, 1998, pp. 183–499.
[23] E. Lee, D. Liu, Finite-strain elastic-plastic theory with application to plane-wave analysis, J. Appl. Phys. 38 (1967).
[24] E. Lee, Elastic plastic deformations at finite strains, Trans. ASME, J. Appl. Mech. 36 (1969).
[25] Z. Cheng, G. Wang, L. Chen, J. Wilde, K. Becker, Viscoplastic Anand model for solder alloys and its application, Solder. Surf. Mount Technol. 12 (2000).
[26] S. Balay, S. Abhyankar, M.F. Adams, J. Brown, P. Brune, K. Buschelman, L. Dalcin, A. Dener, V. Eijkhout, W.D. Gropp, D. Karpeyev, D. Kaushik, M.G. Knepley, D.A. May, L.C. McInnes, R.T. Mills, T. Munson, K. Rupp, P. Sanan, B.F. Smith, S. Zampini, H. Zhang, H. Zhang, PETSc web page, 2019, URL: https://www.mcs.anl.gov/petsc.
[27] S. Balay, S. Abhyankar, M.F. Adams, J. Brown, P. Brune, K. Buschelman, L. Dalcin, A. Dener, V. Eijkhout, W.D. Gropp, D. Karpeyev, D. Kaushik, M.G. Knepley, D.A. May, L.C. McInnes, R.T. Mills, T. Munson, K. Rupp, P. Sanan, B.F. Smith, S. Zampini, H. Zhang, H. Zhang, PETSc Users Manual, Technical Report ANL-95/11 - Revision 3.14, Argonne National Laboratory, 2020, URL: https://www.mcs.anl.gov/petsc.
[28] S. Balay, W.D. Gropp, L.C. McInnes, B.F. Smith, Efficient management of parallelism in object oriented numerical software libraries, in: E. Arge, A.M. Bruaset, H.P. Langtangen (Eds.), Modern Software Tools in Scientific Computing, Birkhäuser Press, 1997, pp. 163–202.
[29] S. Abhyankar, J. Brown, E.M. Constantinescu, D. Ghosh, B.F. Smith, H. Zhang, PETSc/TS: A modern scalable ODE/DAE solver library, 2018, arXiv preprint arXiv:1806.01437.
[30] A. Logg, K.A. Mardal, G.N. Wells (Eds.), Automated solution of differential equations by the finite element method. The FEniCS book, in: Lecture Notes in Computational Science and Engineering, vol. 84, Springer, Heidelberg, 2012.
[31] A. Bermúdez, B. López-Rodríguez, F.J. Pena, R. Rodríguez, P. Salgado, P. Venegas, Numerical solution of an axisymmetric eddy current model with current and voltage excitations, J. Sci. Comput. 91 (8) (2022).
[32] A.F.D. Loula, J. Zhu, Finite element analysis of a coupled nonlinear system, Comput. Appl. Math. 20 (3) (2001) 321–339.